

# Mono-Higgs Signature in the Scotogenic Model with Majorana Dark Matter

Amine Ahriche <sup>a,1,2</sup>, Abdesslam Arhrib <sup>b,3</sup>, Adil Jueid <sup>c,4</sup>,  
Salah Nasri <sup>d,5,2</sup> & Alejandro de la Puente <sup>e,6</sup>

<sup>1</sup>Department of Physics, University of Jijel, PB 98 Ouled Aissa, DZ-18000 Jijel, Algeria.

<sup>2</sup>The Abdus Salam International Centre for Theoretical Physics, Strada Costiera 11, I-34014, Trieste, Italy.

<sup>3</sup>Département de Mathématiques, Faculté des Sciences et Techniques, Université Abdelmalek Essaadi, B. 416, Tangier, Morocco.

<sup>4</sup>INPAC, Shanghai Key Laboratory for Particle Physics and Cosmology, Department of Physics and Astronomy, Shanghai Jiao Tong University, Shanghai 200240, China.

<sup>5</sup>Department of physics, United Arab Emirates University, Al-Ain, UAE.

<sup>6</sup>New York Academy of Science, 7 World Trade Center, 250 Greenwich St. 40th Floor New York, NY 10007-2157, USA.

the date of receipt and acceptance should be inserted later

**Abstract** We study the phenomenology of scotogenic model in the case of Majorana Dark Matter (DM) candidate. This scenario gives important consequences since the parameter space of the model is almost unconstrained compared to the Inert Higgs Doublet Model (or the scotogenic model with scalar DM), and hence, offers new opportunities for discovery at future high energy collider, e.g. the HL-LHC. As an example, we focus on the production of the Standard Model (SM) Higgs boson in association with a pair of dark scalars. Owing to its clean signature, the  $\gamma\gamma$  decay channel of the SM Higgs boson is investigated in great detail at both the HL-LHC (at  $\sqrt{s} = 14$  TeV) and the future FCC-hh (at  $\sqrt{s} = 100$  TeV). After revisiting the LHC constraints from run-II on the parameter space of the model, and selecting benchmark points satisfying all the theoretical and experimental constraints, we found that scalars with mass up to 140 GeV (160 GeV) can be probed at the LHC (FCC-hh) with a  $3 \text{ ab}^{-1}$  of integrated luminosity assuming 5% of uncertainty.

## 1 Introduction

The observation of neutrino oscillations in solar, atmospheric, reactor and accelerator experiments remains one clear indication that the Standard Model (SM) is not a complete framework of fundamental physics. The smallness of the observed neutrino masses tells that at the non-renormalizable level we might not have a straightforward answer to the mechanism that bestows neutrinos with mass. One popular mechanism for generating tiny neutrino mass is the so called seesaw mechanism [1–3]. However, realistic models based on the seesaw mechanism involve high mass scales that are hard to be probed at collider experiments. Neutrino mass generation through loop diagrams is interesting and give *naturally* small masses due to loop-suppression factors. Therefore, these models can be probed at present and future colliders. In these class of models, the smallness of neutrino mass has been addressed within frameworks at one-loop [4, 5], two loops [6–10], three loops [11–26], and four loops [27].

Additionally, experimental evidence of dark matter (DM) has driven many years of investigation shedding light on possible particle and electroweak-size interaction explanations that can reproduce the observed DM relic abundance in the Universe. This paradigm is interesting since it can be tested at colliders such as the Large Hadron Collider (LHC). One of the simplest extensions of the SM consists in incorporating an additional Inert Higgs Doublet  $\Phi$  with a discrete  $Z_2$  symmetry under which the new scalar is odd,  $\Phi \rightarrow -\Phi$ , and the other SM fields even [28]. In this case, the lightest odd particle would act as DM candidate. This model, known as the Inert Higgs Doublet Model (IHDM),

<sup>a</sup>aahrice@ictp.it

<sup>b</sup>aarhrib@gmail.com

<sup>c</sup>adil.jueid@sjtu.edu.cn

<sup>d</sup>snasri@uaeu.ac.ae

<sup>e</sup>lagrange2001@gmail.com

contains one CP-even Higgs identified as the SM Higgs, an other CP-even Higgs  $H^0$ , one CP-odd  $A^0$  and a pair of charged Higgs  $H^\pm$ , and consequently has a rich phenomenology [29–48]. For example, the model provides mono-jet, mono-Higgs, mono-Z, mono-photon signatures that can be tested at the LHC and future colliders. It appears from the above phenomenological studies that the IHDM is strongly constrained from direct and indirect DM searches both for low and intermediate DM masses [39, 49]. For DM lighter than 62.5 GeV, LHC data also puts severe constraints on the invisible decay of the SM Higgs which in turn translate into constraints on a combination of the scalar parameters of the potential [39, 50]. Moreover, collider bounds on the IHDM are obtained as a reinterpretation of neutralinos and charginos pair production both from LEP II [51] and from LHC [52]. From LEP II data, Ref. [51] sets an upper bound on the pseudo-scalar mass,  $m_{A^0}$  (resp  $m_{H^0}$ ), below 100 GeV (resp 80 GeV) consistent with mass splittings  $\Delta m(A^0, H^0) \geq 8$  GeV. While from LHC data, Ref [52] limits have been derived using a dilepton plus missing energy signature which excludes masses for the exotic scalar up to 62.5 GeV. A recent study [50] showed that the LHC at 13 TeV and 3000 fb $^{-1}$  luminosity could exclude exotic scalar masses below 83 GeV using the mono-jet channel.

However, If one focuses on a degenerate spectrum of exotic scalars, which is a natural outcome of accidental symmetries in the scalar potential [53], the region of scalar masses above  $M_Z/2$  remains unconstrained for splittings between the exotic scalar and the charged scalar mass below 5 GeV. It was also found that LHC searches are not strong enough to probe the degenerate window due to lepton  $p_T$  requirements. In the light of current collider experimental bounds and the viable region of parameter space in the IHDM, and in order to address the DM nature, one has to go beyond this minimal extension of the SM. For instance, extending the IHDM by three right handed Majorana fermions may provide a possible solution to the problem of over-constrained quartic couplings and, on the other hand, give rise to small neutrino masses generated through one-loop diagrams. In the present work, we build on a recent phenomenological analysis in the framework of scotogenic model [30] performed by some of us [54]<sup>1</sup>. The scotogenic model is a SM minimal extension where the SM neutrinos obtain naturally small masses at the one-loop order. In order to achieve this, the scalar potential has to be augmented by an inert complex scalar doublet with a small mixing quartic coupling to the SM Higgs. Due to the new Yukawa couplings, the scalar potential has an enhanced  $SU(2)$  symmetry acting only on the exotic scalar and the new right-handed neutrino fields<sup>2</sup>. Because of this global symmetry, the quartic coupling  $\lambda_5$  between  $\Phi$  and the SM Higgs, that is responsible for the mass splitting between the CP-odd and CP-even neutral scalars, does not run and thus can naturally be very close to zero, which naturally yields small mass for the active neutrino. In contrast to the  $\lambda_5$  term in the potential, there is another coupling between  $\Phi$  and the SM Higgs,  $\lambda_4$ , which has non-vanishing  $\beta$ -function even if the coupling is chosen to be zero at some very high energy scale<sup>3</sup>. This region of parameter space corresponds also to a spectrum of a compressed exotic scalar/pseudo-scalar spectrum that leads to interesting collider signatures which are difficult to probe in the IHDM with current and near-future data.

In [54, 55], the DM candidate is considered to be the lightest Majorana fermion  $N_1$ , which implies significant difference in the parameter space compared to both IDHM or the scotogenic model with scalar DM candidate. For instance, in case of scalar DM candidate, the null results from searches in direct detection imply that the coupling combination  $\lambda_L = \lambda_3 + \lambda_4 + \lambda_5$  is extremely suppressed to be suppressed, while for the fermionic DM case this constraint do not affect the scalar potential's parameters. In the fermionic DM case, the CP-odd and CP-even scalars decay predominantly into SM neutrino and the Majorana fermion  $N_i$ , and therefore they can not be seen at colliders, i.e., they behave as dark scalars. In other words, both the IHDM and the scotogenic model provide identical signatures at colliders but with different event yields since they have different parameter space.

As pointed above, the production of dark scalars can lead to several signatures dubbed as mono-X. The most known of and studied in the literature is the mono-jet signature. However, within the framework of scotogenic model, the mono-jet signature is only sensitive to the masses of the particles produced in the final state and not to the scalar couplings such as e.g.  $\lambda_L$ . The reason for this is that the mono-jet cross section gets the most important contribution from diagrams with the exchange of Z-boson and involving *gauge couplings* only. Therefore, alternatives to the mono-

<sup>1</sup>The phenomenology of the scotogenic model has been extensively studied in the literature [56–60].

<sup>2</sup>This symmetry, however, is broken explicitly by the Majorana bare mass terms

<sup>3</sup>Here, one notices that the global  $SU(2)$  is radiatively broken to a global  $U(1)$  that leads to the degeneracy between the CP-odd and CP-even scalars.

jet channel need to be exploited. In this regard, we focus the scope of this work on the mono-Higgs channel in the diphoton final state at both the HL option of the LHC at 14 TeV and a Future Circular Collider (FCC-hh) at 100 TeV. This signature is an excellent probe of new physics and DM [61–64]. We stress out that searches of DM in events with Higgs and missing transverse energy have been carried out by the ATLAS and the CMS collaborations [65–71] using  $\tau^+\tau^-$ ,  $\gamma\gamma$  and  $b\bar{b}$  decay channels of the Higgs boson. These searches yielded null results which were used to put severe constraints on simplified models of DM production at hadron colliders. However, these limits do not apply to our model due to the smallness of the corresponding production cross sections of DM particles in association with a Higgs boson. In this work, we will follow closely the analysis setup of reference [66].

The outline of the paper is as follow. In the second section we review the scotogenic model and all the theoretical and the experimental bounds in the entire degenerate window, where all exotic scalars have approximate equal masses. We then carry out a complete comparison of this model to the latest LHC run II data, and expose the available parameter space in the third section. In the fourth and the fifth sections, we present a full sensitivity analysis to a mono-Higgs signature within this framework.

## 2 The Model: Parameters and Constraints

### 2.1 Model

In this model, the SM is extended by one  $SU(2)_L$  inert Higgs doublet and three singlet Majorana fermions  $N_i \sim (1, 1, 0)$ ,  $i = 1, 2, 3$ . These new particles are odd under a  $Z_2$  symmetry, whereas the SM particles are even. In this setup, the most general gauge-invariant, and renormalizable scalar potential that is invariant under CP- and  $Z_2$ -symmetries has the form

$$V = -\mu_1^2 |H|^2 + \mu_2^2 |\Phi|^2 + \frac{\lambda_1}{6} |H|^4 + \frac{\lambda_2}{6} |\Phi|^4 + \lambda_3 |H|^2 |\Phi|^2 + \frac{\lambda_4}{2} |H^\dagger \Phi|^2 + \frac{\lambda_5}{4} [(H^\dagger \Phi)^2 + h.c.], \quad (1)$$

The electroweak symmetry breaking occurs due to the non vanishing Vacuum Expectation Value (VEV) acquired by the SM Higgs doublet, through its neutral component, while the  $Z_2$ -odd inert doublet  $\Phi$  does not develop a VEV as its quadratic term has positive curvature. The SM Higgs and the inert doublets can be parametrized as

$$H = \begin{pmatrix} G^+ \\ \frac{1}{\sqrt{2}}(v + h + iG^0) \end{pmatrix}, \quad \Phi = \begin{pmatrix} H^+ \\ \frac{1}{\sqrt{2}}(H^0 + iA^0) \end{pmatrix}. \quad (2)$$

The Lagrangian that involves the Majorana fermions can be written as

$$\mathcal{L} \supset h_{ij} \bar{L}_i \epsilon \Phi N_j + \frac{1}{2} M_i \bar{N}_i^C N_i + h.c., \quad (3)$$

where  $\bar{L}_i$  is the left-handed lepton doublet and  $\epsilon = i\sigma_2$  is an antisymmetric tensor. Note that the absence of  $\bar{L}_i H N_j$  in the Lagrangian (3) is due to the imposed discrete  $Z_2$  symmetry. The parameters  $\lambda_1$  and  $\mu_1^2$  in (1) can be eliminated in favor of the SM Higgs mass and its VEV ( $v = 246$  GeV), which is considered at one-loop level à la  $\overline{\text{DR}}$  scheme [72]. After EWSB, three degrees of freedom are absorbed by the longitudinal gauge bosons and we are left with two CP-even scalars ( $h^0, H^0$ ), one CP-odd scalar  $A^0$  and a pair of charged scalars  $H^\pm$ . Their tree-level masses are given by:

$$m_{H^\pm}^2 = \mu_2^2 + \frac{1}{2} \lambda_3 v^2, \quad m_{H^0, A^0}^2 = m_{H^\pm}^2 + \frac{1}{4} (\lambda_4 \pm \lambda_5) v^2. \quad (4)$$

The neutrino mass can be obtained at the one loop level via the diagram in Fig. 2.1. The neutrino mass matrix elements [30, 73] are given à la Casas-Ibarra form [74] by

$$m_{\alpha\beta}^{(\nu)} = \sum_k h_{\alpha k} \cdot G_k \cdot h_{k\beta}^T. \\ G_k = \frac{M_k}{16\pi^2} \left\{ \frac{m_{H^0}^2}{m_{H^0}^2 - M_k^2} \ln \frac{m_{H^0}^2}{M_k^2} - \frac{m_{A^0}^2}{m_{A^0}^2 - M_k^2} \ln \frac{m_{A^0}^2}{M_k^2} \right\} \quad (5)$$

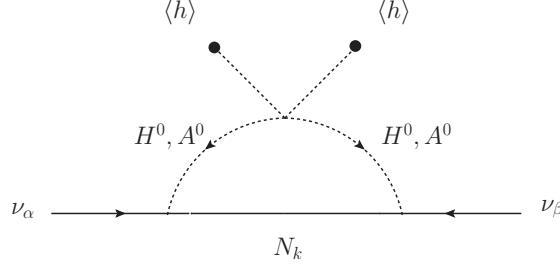


**Fig. 1** Feynman diagram responsible for the neutrino mass.

In this model, the smallness of neutrino mass is a consequence of the tiny mass splitting in the inert neutral sector. In other words, the following ratio  $\epsilon := \frac{|\lambda_5|v^2}{m_{H^0}^2 + m_{A^0}^2}$  is much smaller than unity. Then, after the expansion over  $\epsilon$ , the parameter  $G_k$  in (5) is given by

$$G_k = \frac{|\lambda_5|}{16\pi^2} \frac{v^2}{\bar{m}} \left[ \frac{x_k}{1-x_k^2} + \frac{x_k^3}{(1-x_k^2)^2} \ln x_k^2 \right], \quad (6)$$

with  $x_k = M_k/\bar{m}$  and  $\bar{m}^2 = (m_{H^0}^2 + m_{A^0}^2)/2$ . According to the Casas-Ibarra parameterization, the coupling  $h$  can be written as

$$h = D_{\sqrt{G_k}} \mathcal{R} D_{\sqrt{m_\nu}} U_\nu^\dagger, \quad (7)$$

where  $D_{\sqrt{G_k}} = \text{diag} \{ \sqrt{G_1}, \sqrt{G_2}, \sqrt{G_3} \}$ , and  $D_{\sqrt{m_\nu}} = \text{diag} \{ \sqrt{m_1}, \sqrt{m_2}, \sqrt{m_3} \}$ ,  $\mathcal{R}$  is an orthogonal rotation matrix ( $m_{1,2,3}$  are the neutrino eigenmasses), and  $U_\nu$  is the Pontecorvo-Maki-Nakawaga-Sakata (PMNS) mixing matrix [75]. The parameters of the model are subject to constraints from the measurements of the mixing angles and mass-squared differences [76] which we implement in our analysis.

## 2.2 Constraints

The parameters of the scalar potential have to satisfy a number of theoretical and experimental constraints. On the theoretical side, we should require perturbativity of all the quartic couplings of the scalar fields. In addition, the scalar potential has to be bounded from below in all directions of the field space. For that, the necessary and sufficient conditions are given by [77]

$$\lambda_{1,2} > 0, \quad \lambda_3 + \lambda_4 - |\lambda_5| + 2\sqrt{\lambda_1\lambda_2} > 0, \quad \lambda_3 + 2\sqrt{\lambda_1\lambda_2} > 0. \quad (8)$$

However, these constraints do not ensure the vacuum stability since the inert vacuum may not be the global minimum of the potential, and to guarantee this feature we should also impose the condition  $\frac{\mu_1^2}{\sqrt{\lambda_1}} \geq -\frac{\mu_2^2}{\sqrt{\lambda_2}}$  [78]. Another set of constraints comes from the tree-level perturbative unitarity which should be preserved at high energies in variety of processes involving scalars or gauge bosons. At high energies, using the equivalence theorem, we replace the longitudinal  $W$  and  $Z$  bosons by the corresponding charged and neutral Goldstone bosons respectively. Therefore, we are left only with pure scalar scattering amplitudes. Computing the decay amplitudes for these processes, one finds a set of 4 matrices with quartic couplings as their entries. The eigenvalues for those matrices have to be smaller than  $4\pi$  [79, 80].

Electroweak precision tests (EWPT) is a common approach to constrain physics beyond SM by using the global fit through the oblique  $S$ ,  $T$  and  $U$  parameters [81]. In the scotogenic model, the new gauge-inert interactions will induce non-vanishing contributions to the oblique parameters  $\Delta T$  and  $\Delta S$  [82]<sup>4</sup>. To study the impact of the EWPT

<sup>4</sup>The corrections to the  $U$ -parameter in the IHDM are very small. Therefore, we assume that  $\Delta U = 0$  in the present analysis.

on the mass splitting between the pseudo-scalar ( $A^0$ ) and the charged Higgs boson ( $H^\pm$ ), we have to minimize the function

$$\chi^2 = \sum_{\mathcal{O}=S,T} \frac{(\mathcal{O} - \mathcal{O}_{\text{exp}})^2}{\sigma_{\mathcal{O}}^2(1 - \rho_{ST}^2)} - 2\rho_{ST} \frac{(S - S_{\text{exp}})(T - T_{\text{exp}})}{\sigma_S \sigma_T(1 - \rho_{ST}^2)}, \quad (9)$$

with  $S_{\text{exp}} = 0.06 \pm 0.09$ ,  $T_{\text{exp}} = 0.10 \pm 0.07$  are the experimental values of the  $S$  and the  $T$  parameters,  $\sigma_{S,T}$  are their corresponding errors, and  $\rho_{ST} = +0.91$  is their correlation. The constraints from EWPT can easily be satisfied in regions of the parameter space where the mass splitting between the neutral and the charged components of the inert doublet is small (for light scalars) or where the scalars are very heavy regardless the values of their mass splittings. In this model, constraints from neutrino masses and mixings imply extremely small values of  $\lambda_5$ . Therefore, the only parameter that is directly affected by EWPT constraint is  $\lambda_4$ . This can easily be seen from the left panel of Fig. 2 where we display the 1-, 2- and 3-sigma allowed regions plotted in the  $(m_{H^\pm}, \lambda_4)$  plane. We can see that, for e.g.  $m_{H^\pm} \simeq 95$  GeV,  $\lambda_4$  can vary in  $[-0.2, 1.5]$  which implies a maximum mass splitting of about 100 GeV.

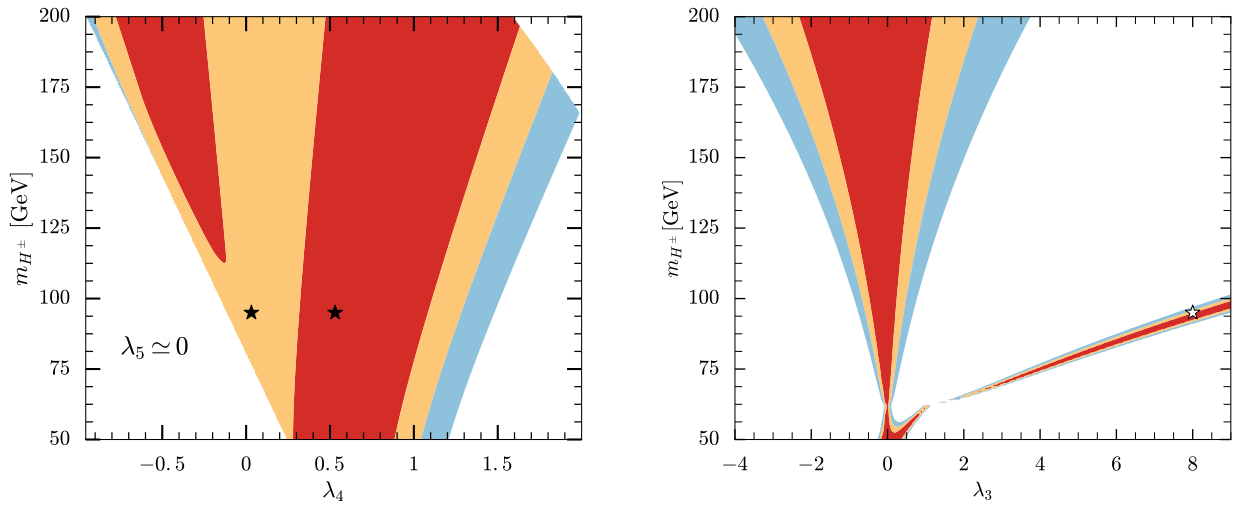


**Fig. 2** Constraints on the model parameter space from oblique parameters in the mass of the charged Higgs mass and  $\lambda_4$  (left) and from Higgs signal strength measurements in the charged Higgs mass and  $\lambda_4$  (right). The red, yellow, and blue contours correspond to the 68%, 95%, and 99.7% allowed regions respectively. Two different benchmark points corresponding to  $(m_{H^\pm}, m_{A^0}) = (95, 100)$  GeV,  $(95, 160)$  GeV are shown as black markers in the right panel. In the right panel, the white marker corresponds to the allowed value of  $\lambda_3$  chosen in the rest of the analysis. Due to the constraints from neutrino mass and mixing parameters, we have taken  $\lambda_5 = 0$ .

Moreover, the gauge bosons decay widths are well measured [83], and must not be modified by any new interactions. Therefore, one needs to impose the conditions  $m_{H^0} + m_{A^0}, 2m_{H^\pm} > M_Z$ ;  $m_{H^\pm} + m_{A^0}, m_{H^\pm} + m_{H^0} > M_W$ , to keep the decay channels of  $W$  and  $Z$  gauge bosons into inert particles closed.

The new Yukawa interactions in (3) lead to lepton flavor violating (LFV) decay processes that arise at one-loop level with the exchange of charged Higgs  $H^\pm$  and Majorana fermions  $N_k$  particles. The branching ratio of the decays  $\ell_\alpha \rightarrow \ell_\beta + \gamma$  and  $\ell_\alpha \rightarrow \ell_\beta \ell_\beta \ell_\beta$  are given in the literature [84], and should be in agreement with the available experimental constraints [83].

In the scotogenic model, all the SM Higgs couplings with SM particles are the same as in the SM except those relevant to the decays  $H \rightarrow \gamma\gamma$  and  $H \rightarrow \gamma Z$  which receives additional contributions from the charged Higgs bosons. Therefore, in the case where there is no large contribution to the invisible decay of the SM Higgs, most of the LHC measurements would fit pretty well within the scotogenic model. This is the case in our model, the only source of invisible decay is the one-loop induced coupling  $HN_i N_j$  which is suppressed in most regions of the parameter space. In the scotogenic model, the partial width of the SM Higgs boson in the  $\gamma\gamma$  channel depends on the charged Higgs boson mass and  $\lambda_3$ . Positive (negative) values of the  $\lambda_3$  would imply destructive (constructive) interferences with

the leading  $W$  and the sub-leading top quark contributions [42]. Since the charged Higgs  $H^\pm$  contribution would modify the rate of through  $H \rightarrow \gamma\gamma$ , we need to check the constraints on the parameter space from diphoton signal strength measurements at the LHC. The public package LILITH [86, 87] was used to check the constraints from various measurements of the Higgs boson signal strength ( $\mu_{\gamma\gamma}^i$ ) defined by

$$\mu_{\gamma\gamma}^i = \frac{\sigma^i \Gamma(H \rightarrow \gamma\gamma)}{\sigma_{\text{SM}}^i \Gamma(H \rightarrow \gamma\gamma)^{\text{SM}}}, \quad (10)$$

with the superscript  $i$  refers to the production channel of the SM Higgs boson. In the right panel of Fig. 2, we plot the allowed regions from Higgs boson signal strength measurements in the  $(\lambda_3, m_{H^\pm})$  plane. We can see that  $\mu_{\gamma\gamma}$  constrains strongly the 2D parameter space. There are two notable regions for  $m_{H^\pm} < 125$  GeV; the first one is centered around  $\lambda_3 \simeq 0$  while the second one is a small segment corresponding to  $\lambda_3 \in [0, 9]$  and  $m_{H^\pm} < 100$  GeV. This unsurprising because even for large positive values of  $\lambda_3$ , the  $R_{\gamma\gamma}$  ratio in our model can still agree with data within the +10% of experimental uncertainty reported in e.g. the recent CMS analysis [88].

In this study, we assume that the lightest right-handed Majorana neutrino is a DM candidate as was done in ref [54]. For light Majorana neutrinos (with masses up to 140 GeV) that we are interested in, the main annihilation channels are into charged leptons and SM neutrinos. These annihilation processes proceed through  $t$ -channel diagrams mediated by the members of the inert doublet. Furthermore, in the aim of simplifying the collider analysis (see sections 3 and 4), nearly degenerate Majorana neutrinos are chosen, i.e  $m_{N_2} \simeq 1.01m_{N_1}$  and  $m_{N_3} \simeq 1.02m_{N_1}$ . In this case, co-annihilation becomes important and, therefore, is included in our analysis. Co-annihilation with inert scalars, which give rise to final states such as  $\ell^\pm \gamma$ , is sub-leading due to the smallness of the electromagnetic coupling compared to the new Yukawa couplings  $h_{ik}$  and can be safely neglected. Including all the significant channels, we select a benchmark point that is in agreement with the WMAP [89] and PLANCK [90] measurements of the relic density at the  $2\sigma$  level.

In our model, DM can interact with the nucleons and triggers a possible signal in direct detection experiments. This can happen despite the absence of a tree level  $HN_1N_1$  coupling which arises at the one-loop order. We estimated spin-independent (SI) scattering cross section of  $N_1$  off a nucleon  $\mathcal{N}$  and subject it to constraints from the searches performed by XENON1T [91]. One notices that constraints from direct detection are easily satisfied in our model due to the smallness of  $HN_1N_1$  coupling. We refer the reader to [54] for more details about the DM constraints in our model.

### 2.3 LEP constraints

Multiple searches for supersymmetric particles at  $e^+e^-$  collisions has been carried out by several collaborations [92–95] for center-of-mass energies of 183-209 GeV. The searches focused on charginos and neutralinos pair production in events with two or three leptons and large transverse missing energy. Several interpretations in terms of models containing charged and neutral scalars have been made. Ref. [51] made a comprehensive re-interpretation of neutralino pair production ( $\chi_1^0\chi_2^0$ ) to constrain the production of  $H^0A^0$  in the IHDM and got a limit  $m_{A^0} > 100$  GeV for large mass splitting. Pair production of charginos ( $\chi_1^+\chi_1^-$ ) was analyzed to put constraints on  $H^\pm H^\mp$  production in a DM model with TeV scale colored particles [96] and in the compressed IHDM [53].

In this section, we study the impact of LEP searches on the parameter space of our model. For instance, LEP put strong bounds on the pair production cross section of lightest neutralino. However, the LEP limits on neutralino pair production do not apply in the considered scenario of the scotogenic model, because the tiny value of the coupling  $\lambda_5$  (of order  $10^{-8}$ - $10^{-10}$ ) required by the smallness of neutrino masses forbids off-shell decays, such as  $A^0 \rightarrow H^0 Z \rightarrow H^0 \ell\ell$ , and therefore yields an undetected final state. However, limits from chargino pair production can be applied to our model. Two processes can be used for such constraints;  $e^+e^- \rightarrow H^+H^-$  and  $e^+e^- \rightarrow H^0A^0$ . The latter contribute, if  $\lambda_4 < 0$  and  $\Delta_{H^\pm H^0} = m_{A^0, H^0} - m_{H^\pm} > m_{e, \mu}$ , through off-shell decays. This contribution is proportional to  $(\Delta_{H^\pm H^0})^5$  and, hence, is very small. Therefore, charged Higgs pair production is the only process to

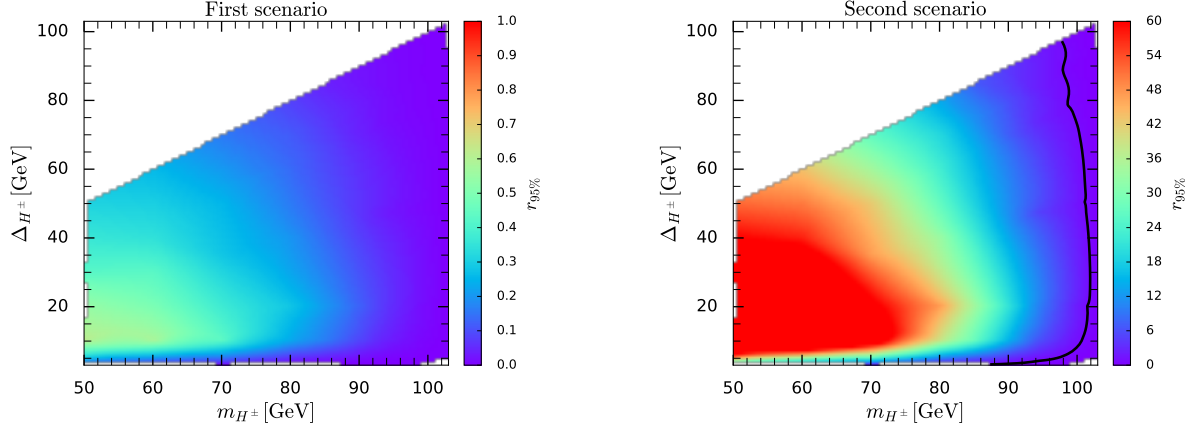


**Fig. 3** Results of re-interpretation of LEP searches of chargino pair production on the  $(\Delta_{H^\pm}, m_{H^\pm})$  plan in the first scenario (*left*) and second scenario (*right*).

which the exclusion limits from LEP searches can be used to constrain our model. We consider the results of searches carried by OPAL [94] at  $\sqrt{s} = 208$  GeV and  $\mathcal{L} = 680 \text{ pb}^{-1}$  of integrated luminosity to derive conservative limits on the model parameter space i.e. by assuming that the efficiency of the selection is 100%<sup>5</sup>

The pair production of the charged particle depends on new Yukawa couplings and the gauge couplings. The first contribution is proportional to

$$\sum_{k=1}^3 |h_{ek}|^2 = |h_{e1}|^2 + |h_{e2}|^2 + |h_{e3}|^2, \quad (11)$$

in the case of degenerate Majorana fermions. Because, for  $\lambda_4 \geq 0$ , the Charged Higgs boson decays with 100% branching ratio into  $N_k \ell$ , the limits from charginos searches can be used to constrain both the charged Higgs boson and the mass splitting  $\Delta_{H^\pm}$  defined by

$$\Delta_{H^\pm} = m_{H^\pm} - m_{N_1}. \quad (12)$$

We consider two scenarios for the new Yukawa couplings; 1) where the Yukawa matrix is chosen as follows

$$\frac{h_{ij}}{10^{-2}} = \begin{pmatrix} -60.86 - i0.20 & -0.30 - i0.80 & 14.49 - i0.75 \\ 25.14 - i0.57 & -1.12 - i2.49 & 40.87 + i0.24 \\ 3.70 + i0.62 & 1.10 + i3.88 & -44.20 + i0.14 \end{pmatrix} \quad (13)$$

which we called first scenario and 2) the second scenario where the  $h_{ek}$  couplings take the highest values allowed by all the theoretical and experimental constraints ( $h_{e1} = -0.026 + i0.042$ ,  $h_{e2} = 2.22 - i0.081$ ,  $h_{e3} = 0.32 - i0.0098$ ). In the second scenario, the most important contribution comes from  $|h_{e2}|$ .

We estimate the  $r_{95\%}$  ratio defined by

$$\begin{aligned} r_{95\%} &= \frac{\sigma(e^+e^- \rightarrow H^+H^-) \times (\text{BR}(H^\pm \rightarrow N_k \ell^\pm))^2}{95\% \sigma(e^+e^- \rightarrow \chi_1^+ \chi_1^-) \times (\text{BR}(\chi_1^\pm \rightarrow \chi_1^0 \ell^\pm \nu_\ell))^2} \\ &= \frac{\sigma(e^+e^- \rightarrow H^+H^-)}{95\% \sigma(e^+e^- \rightarrow \chi_1^+ \chi_1^-) \times (\text{BR}(\chi_1^\pm \rightarrow \chi_1^0 \ell^\pm \nu_\ell))^2}, \end{aligned} \quad (14)$$

where, in the second line of eq. (14), we used  $\text{BR}(H^\pm \rightarrow \ell^\pm N_k) = 1$ . A point in the parameter space is excluded if the corresponding  $r_{95\%}$  is larger than 1. In Fig. 3, we depict the exclusions from charginos pair production on the  $(m_{H^\pm}, \Delta_{H^\pm})$  plan. As can be seen from the left panel of Fig. 3, all points are allowed by LEP searches. However, in the second scenario, one notices that the model is excluded for  $m_{H^\pm} < 100$  GeV. A small window corresponding to  $\Delta_{H^\pm} < 5$  GeV and  $90 \text{ GeV} < m_{H^\pm} < 100 \text{ GeV}$  is still allowed by these constraints.

<sup>5</sup>Full analysis of the signal process at the detector level will yield to an efficiency that is always smaller than 100%. Therefore, the limits we obtain in this study are more conservative.



### 3 Constraints from LHC searches at 13 TeV

The model parameter space can be constrained by re-interpreting several ATLAS and CMS searches for new physics beyond the SM. In this study, we used the public tool CHECKMATE [109–113] which is dedicated for re-interpretation of LHC searches of new physics. Degenerate Majorana neutrinos are chosen to avoid the possibility for displaced vertices. The other parameters are fixed to avoid all the other theoretical and experimental constraints [54] and they are chosen to be

$$\lambda_3 = 8, \quad m_{H^\pm} = 95 \text{ GeV and } m_{A^0} \in [100, 200] \text{ GeV.} \quad (15)$$

The LHC searches used in this analysis are displayed in Table 1. The model parameter space can be affected by the LHC searches displayed in Table 1 as we will show explicitly. Details about the different searches performed at the LHC and the model-dependent processes that are sensitive to them are reported in Appendix A.

In our model, new sources of missing transverse energy,  $E_T^{\text{miss}}$ , namely from right-handed neutrinos,  $N_i$  exist. These new sources can be probed at colliders with events triggered by large missing  $E_T^{\text{miss}}$ . However, Majorana neutrinos cannot be produced directly because of the absence of the vertices  $Z^0 N \bar{N}$ ,  $\gamma N \bar{N}$ , and  $H N \bar{N}$ ; right-handed neutrinos are thus produced via the decays of the exotic scalars.

**Table 1** Selected set of ATLAS and CMS searches that were used in the re-interpretation study. These analyses are implemented in CHECKMATE.

Analysis	Experiment	Luminosity ( $\text{fb}^{-1}$ )	Reference
atlas_conf_2016_050	ATLAS	13.3	[97]
atlas_conf_2016_066	ATLAS	13.3	[98]
atlas_conf_2016_076	ATLAS	13.3	[99]
atlas_conf_2017_060	ATLAS	36.1	[100]
atlas_1704_03848	ATLAS	36.1	[101]
atlas_1709_04183	ATLAS	36.1	[102]
atlas_1712_02332	ATLAS	36.1	[103]
atlas_1712_08119	ATLAS	36.1	[104]
atlas_1802_03158	ATLAS	36.1	[105]
cms_sus_16_025	CMS	12.9	[106]
cms_sus_16_039	CMS	35.6	[107]
cms_sus_16_048	CMS	35.9	[108]

In the degenerate window, since the decay  $A^0 \rightarrow H^0 Z^0$  is kinematically forbidden, the scalar/pseudoscalar can be produced in association with a charged scalar which subsequently decays to a charged lepton and a right-handed neutrino. While the scalar and pseudoscalar may only decay invisibly; we obtain a signal with a single lepton and large missing  $E_T^{\text{miss}}$ . In this channel the most sensitive LHC search comes from the work in [97] that searches for SUSY in a final state with one isolated lepton. In the case where the exotic scalars are pair produced, in the degenerate region, their decays lead only to missing  $E_T^{\text{miss}}$  and one can tag this channel with a mono-jet from initial state radiation. In these cases, LHC searches with photons and jets are the most sensitive, with the largest amount of missing  $E_T^{\text{miss}}$  when the scalar/pseudoscalar mass approaches the right-handed neutrino mass, and this is where the bulk of the exclusion lies in as can be seen from Figure 4 after the inclusion of all relevant LHC searches given in Table 1. Following the results of the re-interpretation of LHC searches of new physics that we have shown in Fig. 4, we choose the following benchmark points for the mono-Higgs study;

$$100 \text{ GeV} \leq m_{H^0} = m_{A^0} \leq 200 \text{ GeV}, \quad m_{H^\pm} = 95 \text{ GeV} \\ m_{N_1} = m_{N_2} = m_{N_3} = 80 \text{ GeV}, \quad \lambda_3 = 8. \quad (16)$$



while the new Yukawa couplings are fixed to their values shown in eq.(13).

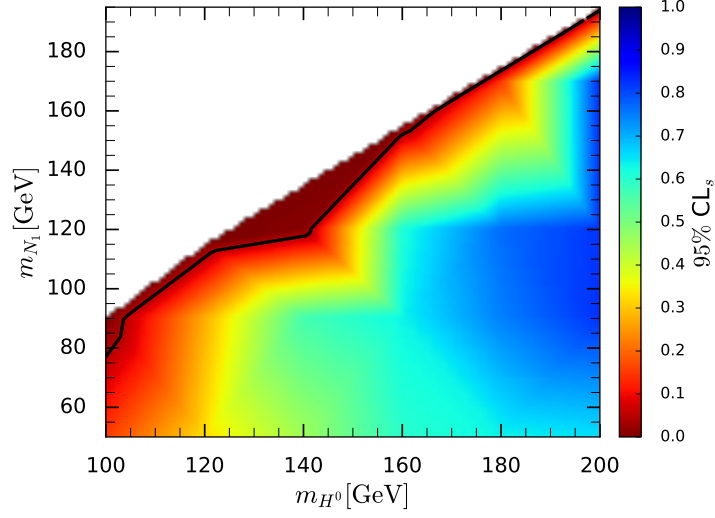


**Fig. 4** Exclusions from LHC searches for new physics at  $\sqrt{s} = 13$  TeV projected on the  $(m_{H^0}, m_{N_1})$  plan. The color map shows the  $CL_s$  values. The black line shows the excluded regions corresponding to  $CL_s < 0.05$  while the white shaded area shows the region that is forbidden by the constraint  $m_{H^0} > m_{N_1}$ .

#### 4 Mono-Higgs signature

In this section, we describe different aspects of our analysis. First we discuss the contribution to the signal process as well as the possible backgrounds and the corresponding cross sections. Then, we discuss in depth the phenomenological setup used in our analysis and event selection.

##### 4.1 Signal and backgrounds

In this model, mono-Higgs production proceeds through two different processes, i.e

$$pp \rightarrow SSH \rightarrow N_i N_j \nu \bar{\nu} H \quad (17)$$

and

$$pp \rightarrow N_i N_j H. \quad (18)$$

The corresponding Feynman diagrams are depicted in Fig. 5. There are four contributions to Higgs+ $E_T^{\text{miss}}$  signal in hadronic collisions which involve either the production of an off-shell Higgs boson or a  $Z$ -boson. In the first diagram (5-a), the off-shell Higgs boson splits into  $SSH$  while in the second one, it involves a contribution from the SM Higgs trilinear coupling  $\lambda_{HHH}$  (5-b). In the third contribution (5-c),  $q\bar{q}$  annihilates into a  $Z^*$  which splits into two dark Higgses. The fourth contribution consists of two Majorana neutrinos produced in association with a SM Higgs boson (5-d). The first and second contributions interfere destructively (constructively) for negative (positive) values of the  $HSS$  couplings. We notice that the contribution of diagram-c is the most dominant one as it contributes about 95%

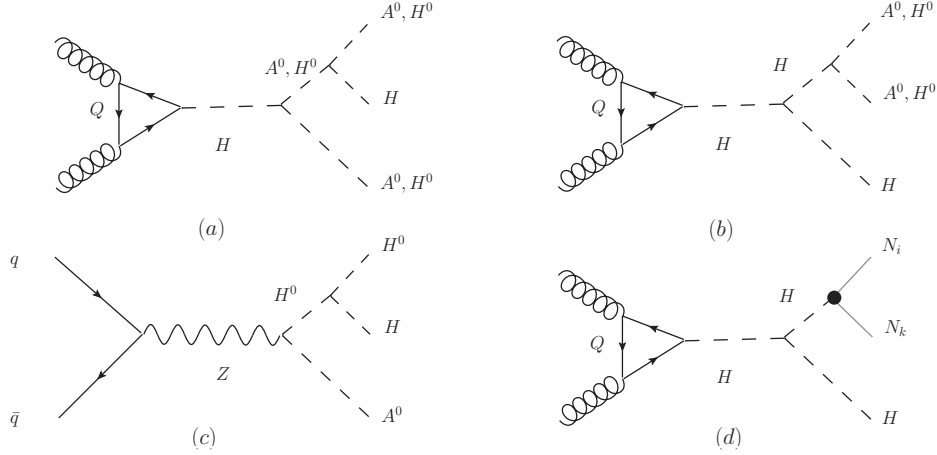


**Fig. 5** Parton level Feynman diagrams contributing to the mono-Higgs signal in hadronic collisions. Unlike the fourth diagram, the first three diagrams are efficient only when the decays  $H^0/A^0 \rightarrow W^\pm H^\mp$  have extremely small branching fractions.

of the total cross section. This is unsurprising since this contribution occurs at the tree level and is enhanced for large values of  $\lambda_L$ . Using simple power counting, one notices that the total cross section behaves as

$$\sigma \propto \left| \lambda_L^2 \mathcal{M}_a + \lambda_L \lambda_{HHH} \mathcal{M}_b \right|^2 + \left| \lambda_L \mathcal{M}_c \right|^2 + \left| \sum_{i,j=1}^3 \tilde{y}_{HN_i N_j} \lambda_{HHH} \mathcal{M}_d \right|^2. \quad (19)$$

The contribution of diagram 5-d is proportional to the squared of the  $HN_i N_j$  coupling which is one-loop induced [54] and it is expected to be very small. In this regard, we define the ratio  $\mathcal{R}$  by

$$\mathcal{R} = \frac{\sum_{i,j=1}^3 |\tilde{y}_{HN_i N_j}|^2}{|\lambda_L|^4}, \quad (20)$$

which gives a rough estimate of the relative contribution of diagram 5-d to the signal cross section where only the leading contribution to  $SSH$  production ( $\simeq |\lambda_L|^4$ ) is included. We show this ratio in Fig. 6 as function of the mass splitting  $\Delta m_{NH^0} = m_{H^0} - m_{N_k}$  with a color map showing  $|\lambda_3|$ . One can see that this ratio can only be important for very small values of  $\lambda_L$ , i.e  $|\lambda_L| < 0.1$ . Given that this region is not interesting from phenomenological point of view as it yields very small cross sections (see Fig. 7), we conclude that the contribution of diagram (5-d) can be safely neglected.

The cross sections for the mono-Higgs production are depicted in the left panel of Fig. 7. As expected, one can see that the cross section is pretty small for the LHC at  $\sqrt{s} = 14$  TeV with the maximum being  $\sigma_{\max} \simeq 53$  fb for  $m_{H^0} = 100$  GeV which increases by about an order of magnitude at the FCC-hh with 100 TeV. Since the mass splitting  $\Delta m_{H^\pm H^0}$  can be as large as 100 GeV, the dark neutral (pseudo)-scalar does not always decay exclusively into an invisible final state. Therefore, in order to estimate correctly the number of events in a signal benchmark point, one has to scale correctly the corresponding cross section by  $\text{BR}(H^0 \rightarrow \text{invisible})^2$ . We show the Dark scalar branching ratios as a function of  $m_{H^0}$  in Fig. 7 (right). We can see that, unless  $m_{H^0} > 190$  GeV, the invisible decays of  $H^0$  have always a branching fraction larger than 90%.

The  $\gamma\gamma$  decay channel represents a very clean signature of the mono-Higgs final state boson despite the smallness of the corresponding branching ratio (which is about  $\simeq 0.23\%$ ). In this case, the following backgrounds have to be considered

- $gg \rightarrow H \rightarrow \gamma\gamma$ : this is the dominant background. The missing energy is due to the mis-identification of soft QCD radiation. However, it can be substantially suppressed by requiring high missing transverse energy as we will show later on.
- $pp \rightarrow ZH$ : where the  $Z$ -boson decays to a pair of neutrinos is an irreducible background. The suppression of this background can be achieved by applying specific selection criteria, e.g on the transverse mass of the (Higgs,  $E_T^{\text{miss}}$ ) system.

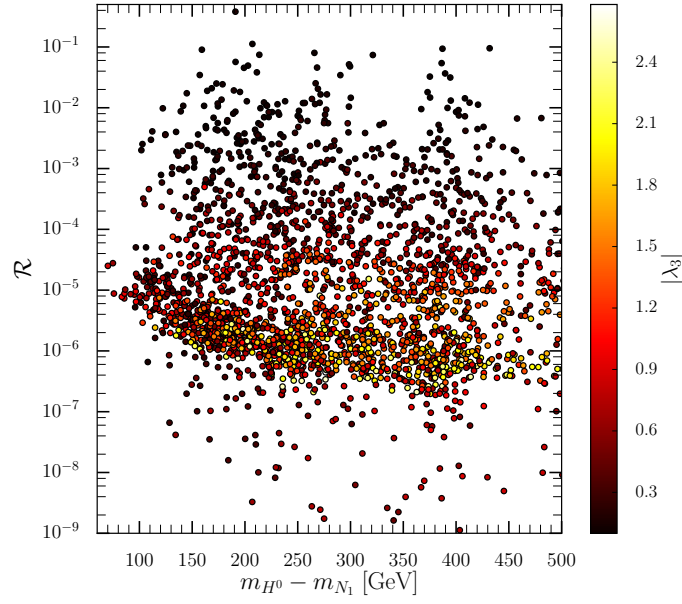


**Fig. 6**  $\mathcal{R}$ , defined in eq. (20), as a function of  $m_{H^0} - m_{N_1}$ . The color map shows the values of  $|\lambda_L|$ . The points shown in the plot satisfy all the theoretical and experimental constraints discussed in section 2.

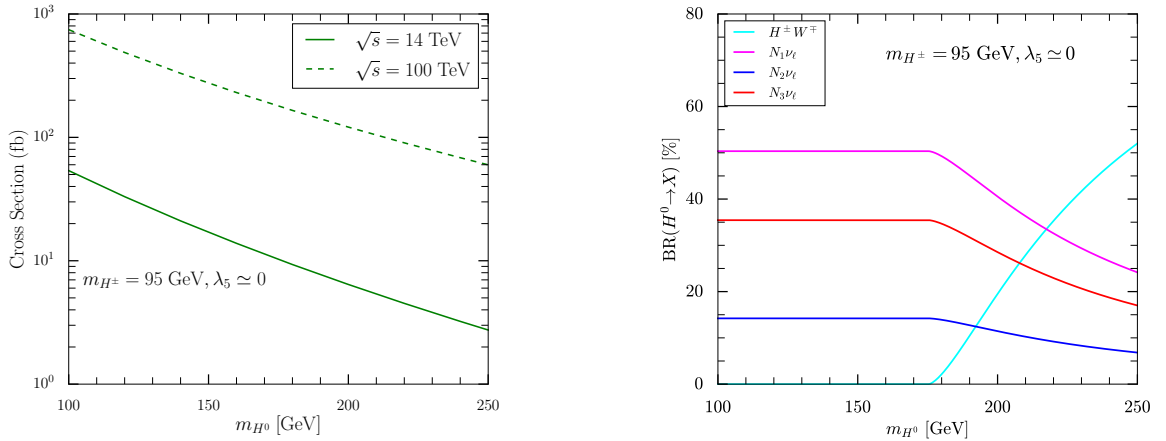


**Fig. 7** *Left*: Mono-Higgs boson production cross section as a function of the Dark scalar mass  $m_{H^0} \simeq m_{A^0}$  for  $m_{H^\pm} = 95$  GeV at the LHC (solid line) and at a future 100 TeV collider (dashed). We included the processes  $gg \rightarrow H^0 H^0 H$ ,  $gg \rightarrow A^0 A^0 H$  and  $q\bar{q} \rightarrow H^0 A^0 H$ . The depicted results were computed LO with MADGRAPH5\_AMC@NLO. *Right*: Decay branching ratios of the Dark scalar particle as a function of the Dark scalar mass.

- $pp \rightarrow W^\pm H$ : where the  $W^\pm$ -boson decays into  $\ell^\pm \nu$  where the charged lepton escapes the detection, i.e not passing the selection threshold. At the LHC, the charged lepton efficiency is high and, therefore, we expect that this background will have small contribution.
- $pp \rightarrow V\gamma\gamma$ : where the  $V = Z$ -boson decays invisibly and the  $V = W$ -boson decays leptonically. The  $Z\gamma\gamma$  background is irreducible contrarily to the  $W\gamma\gamma$ . The contribution of the latter can be reduced by imposing a lepton veto in the selection procedure. Both the two backgrounds have weaker  $\gamma$  spectrum and, therefore, their contribution can be weakened by strong requirements on the  $p_T^\gamma$  and the invariant mass of the  $\gamma\gamma$  spectrum.
- $pp \rightarrow V\gamma$ : this background is similar to  $V\gamma\gamma$ .

**Table 2** Cross sections for processes contributing to the Higgs+ $E_T^{\text{miss}}$  background. The numbers outside (inside) the brackets refers to the rates at 14 (100) TeV. Details about the computation are explained in the text. Here,  $\sigma \times \text{BR}$  refers to  $\sigma(gg \rightarrow H) \times \text{BR}(H \rightarrow \gamma\gamma)$  for  $gg \rightarrow H$ , and to  $\sigma(pp \rightarrow ZH) \times \text{BR}(H \rightarrow \gamma\gamma) \times \text{BR}(Z \rightarrow \bar{\nu}_\ell \nu_\ell)$  for  $ZH$ , to  $\sigma(pp \rightarrow W^\pm H) \times \text{BR}(H \rightarrow \gamma\gamma) \times \text{BR}(W^\pm \rightarrow \ell^\pm \nu_\ell)$  for the case of  $W^\pm H$  and to  $\sigma(pp \rightarrow W^\pm + n\gamma) \times \text{BR}(W^\pm \rightarrow \ell^\pm \nu_\ell) + \sigma(pp \rightarrow Z + n\gamma) \times \text{BR}(Z \rightarrow \bar{\nu}_\ell \nu_\ell)$  for  $V + n\gamma, n = 1, 2$ .

Process	$\sigma \times \text{BR}$ [fb]	Generator	Perturbative Order
$gg \rightarrow H$	128.54 ( $1.94 \times 10^3$ )	SUSHI [114, 115]	NNLO
$W^\pm H$	1.16 (12.59)	VH@NNLO [116]	NNLO
$ZH$	0.52 (7.34)	VH@NNLO [116]	NNLO
$V\gamma\gamma$	51.99 (621.96)	MADGRAPH5_AMC@NLO [117]	NLO
$V\gamma$	$42.89 \times 10^3$ ( $397.04 \times 10^3$ )	MADGRAPH5_AMC@NLO [117]	NLO
$\gamma\gamma + \text{jets}$	$4.19 \times 10^6$ ( $52.81 \times 10^6$ )	SHERPA [118]	NLO

- $pp \rightarrow \gamma\gamma + \text{jets}$ : In the hadronic environment, there is a possibility that pile-up events will contribute to fake high missing transverse energy. The rate of this process is very high and we opt to generate parton level cross sections with some cuts on the  $p_T$  of photons and jets. ATLAS [66] and CMS [71] collaborations used different strategies to reduce the contribution of this background either by defining some kinematical variables or use azimuthal separation between the reconstructed Higgs candidate and the missing transverse energy. These features will be discussed briefly in the next subsection.

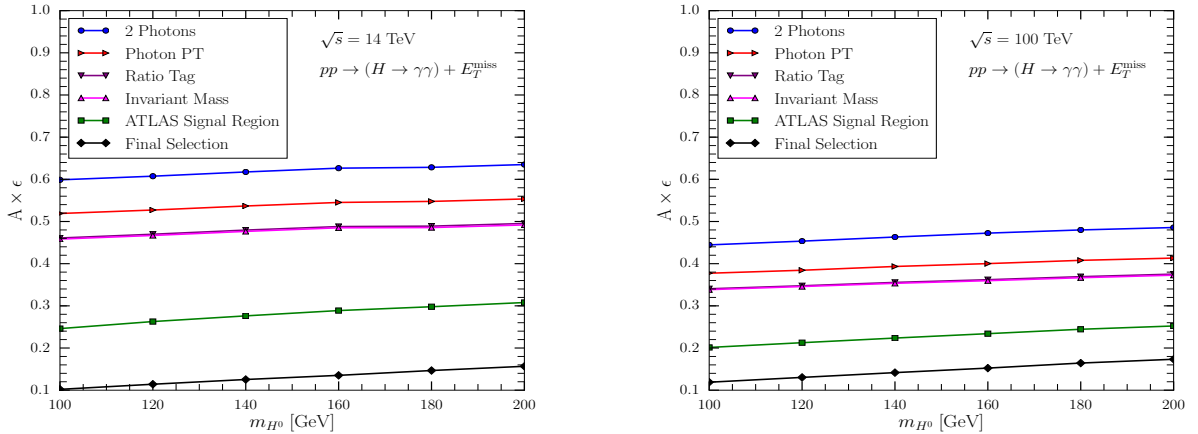


**Fig. 8** The acceptance times the efficiency ( $A \times \epsilon$ ) for the signal after each step of the event selection as a function of the dark Higgs mass for  $\sqrt{s} = 14$  TeV (left) and  $\sqrt{s} = 100$  TeV (right). We show  $A \times \epsilon$  after the "2 Photons" selection step (blue), for the events passing the "Photon PT" selection (red), after the photon isolation selection denoted by "Ratio Tag" (purple) and for events in which the invariant mass of the diphoton system falls in the interval  $m_{\gamma\gamma} \in [110, 160]$  GeV (rose). The efficiency for the two signal regions are shown in green (ATLAS signal region) and in black (tight selection).

#### 4.2 Phenomenological setup and Event selection

The cross sections of the background processes are depicted in Table 2 for both the LHC at  $\sqrt{s} = 14$  TeV and FCC-hh at  $\sqrt{s} = 100$  TeV. The cross section of  $gg \rightarrow H$  was computed at NNNLO using SUSHI [114, 115] version 1.6.1 which implements the results of [119–123]. The rates for  $W^\pm H$  and  $ZH$  processes were estimated at NNLO [120, 124] including NLO EW corrections [125] and top quark mass effects [126] using the public package VH@NNLO [116] version 2.0.3. In all the NNLO calculations, the CT10 PDF set [127] was used with  $\alpha_s(M_Z^2) = 0.118$ . The cross section for  $V\gamma$  and  $V\gamma\gamma$  was evaluated at NLO using MADGRAPH5\_AMC@NLO [117] with the NNPDF30 PDF sets [128]. The

**Table 3** Cut flow for  $H \rightarrow \gamma\gamma$  final state at the LHC at  $\sqrt{s} = 14$  TeV and for  $3 \text{ ab}^{-1}$  of luminosity.

Cuts	SM Higgs	$V\gamma\gamma, V\gamma$	$\gamma\gamma$ +jets	Signal	$S/B$
Initial events	322359	128432167	24030000	365	$2.4 \times 10^{-6}$
2 Photons	168005	2548352	6837913	218	$2.3 \times 10^{-5}$
Photon PT	150570	1177335	6317283	189	$2.5 \times 10^{-5}$
Ratio Tag	135720	830147	5582001	168	$2.6 \times 10^{-5}$
Invariant Mass	135492	174358	2066511	166	$6.9 \times 10^{-5}$
ATLAS Signal Region	98	151	0	89	0.35
Final Selection	29	5	0	32	0.94

**Table 4** Cut flow for  $H \rightarrow \gamma\gamma$  final state at the LHC at  $\sqrt{s} = 100$  TeV and for  $3 \text{ ab}^{-1}$  of luminosity.

Cuts	SM Higgs	$V\gamma\gamma, V\gamma$	$\gamma\gamma$ +jets	Signal	$S/B$
Initial events	5885817	1192995664	252090000	5147	$3.5 \times 10^{-6}$
2 Photons	2597337	18298491	73202377	2287	$2.4 \times 10^{-5}$
Photon PT	2272845	8405387	67325991	1941	$2.5 \times 10^{-5}$
Ratio Tag	2051298	6134810	59189681	1753	$2.6 \times 10^{-5}$
Invariant Mass	2048497	1228567	21714801	1741	$6.9 \times 10^{-5}$
ATLAS Signal Region	4882	1889	0	1036	0.15
Final Selection	2215	315	0	612	0.24

estimate of  $\gamma\gamma$  process (excluding  $H$  contribution) was done using SHERPA version 2.2.5 [118] where inclusive samples of multiplicity up to 4 jets in the final state are merged using the CKKW matching scheme [129] and a merging scale  $Q_0 = 20$  GeV.

Events for both the signal and the backgrounds were generated using MADGRAPH5\_AMC@NLO and PYTHIA8 [130] at LO in QCD. Background events involving the Higgs boson were generated and decayed with PYTHIA8 while  $V\gamma$  and  $V\gamma\gamma$  events were generated using MADGRAPH5\_AMC@NLO including the leptonic decays of the massive electroweak gauge bosons. The  $\gamma\gamma$ +jets events were generated with PYTHIA and normalized to their rate at NLO. Since the rate of this process is huge, and most of the events will be vetoed in the initial selection, events are generated with a  $p_{T,\gamma}^{\min} = 70$  GeV, and  $|\eta^\gamma| < 2.5$ . Events for  $gg \rightarrow H$  were scaled by a  $K$ -factor of 3.2 using the results of SUSHI while  $VH$  events were scaled by a factor of 1.6. All the background events were showered with PYTHIA. DELPHES3 was used for fast detector simulation [131].

The analysis of events was carried out at the detector level using implemented efficiencies, and mis-identification rates in DELPHES where the parameters are tuned for the ATLAS experiment and extrapolated for a future FCC-hh [132]. Events pass a preselection stage with all the objects (leptons, jets, photons and missing  $E_T$ ) are kept. The Acceptance times the efficiency ( $A \times \epsilon$ ) is depicted in Fig. 8 as function of  $m_{H^0}$  for  $\sqrt{s} = 14$  TeV and  $\sqrt{s} = 100$  TeV. The cutflow for the event selection is shown in Tables 3 and 4. Events are selected if they contain at least two photons with  $p_T^\gamma > 25$  GeV and  $|\eta^\gamma| < 2.37$ . This selection is denoted by "Photon PT" in Fig. 8 and Tables 3 and 4. Besides, we do not impose any requirement on the multiplicity, hardness and flavor compositions of jets or the multiplicity of charged leptons. The photons that pass the initial selection will be subject to further isolation cuts (as in [66]), and the photon candidates are ordered by their transverse momentum. The two leading photons are used to reconstruct a *Higgs candidate*. Further, The ratio of the transverse momentum to the invariant mass  $p_T^\gamma/m_{\gamma\gamma}$  is required to be larger than 0.35 (0.25) for the leading (sub-leading) photon. Furthermore, a cut on the invariant mass of the diphoton system is imposed; namely events are selected if  $110 \text{ GeV} < m_{\gamma\gamma} < 160 \text{ GeV}$ . But in some cases, events in the  $\gamma\gamma$  and  $\gamma$ +jets backgrounds contain large fake transverse missing energy, which is due to the fact that, in such events, the vertex with larger  $\sum p_T^2$  (where the sum runs over all the tracks) is not the primary vertex but the one coming from

pile-up.<sup>6</sup> Both ATLAS and CMS collaborations used sophisticated methods to reduce the contribution of pile-up to missing transverse energy. The ATLAS collaboration has defined a new variable  $S_{E_T^{\text{miss}}}$  defined by

$$S_{E_T^{\text{miss}}} = \frac{E_T^{\text{miss}}}{\sqrt{\sum_i E_T^i}}, \quad (21)$$

where  $i$  correspond to all the objects (photons, jets, and leptons) used to construct the missing transverse energy. Besides, to improve the resolution of the  $E_T^{\text{miss}}$ , tracks and clusters not associated to the diphoton primary vertex are not used to reconstruct  $E_T^{\text{miss}}$  [66]. The CMS collaboration used variables that characterize the back-to-back event topology of the signal events (for instance  $|\Delta\Phi(E_T^{\text{miss}}, \mathbf{p}_{\gamma\gamma})|$ ). By requiring that such quantity is larger than 2.1, only events where the reconstructed Higgs and missing transverse energy are back-to-back are selected. Therefore, the contribution from e.g.  $\gamma\gamma$  backgrounds is significantly reduced.

We compared between the approaches used by ATLAS and CMS to reduce the contribution from  $\gamma\gamma$ +jets backgrounds, on our benchmark points; and we found that they produce results that agree with each other. We will follow the ATLAS selection criteria throughout this study. We define two signal regions; the mono-Higgs signal region (denoted by ATLAS signal region in this paper) and a tight signal region. The kinematical quantities and selection rules are displayed in Table 5. In the two signal regions, we require that the invariant mass of the diphoton system falls inside the interval [115, 135] GeV. Furthermore, we require that events contain no lepton (either electron or muon) with  $p_T^\ell > 10$  GeV and  $|\eta^\ell| < 2.5$ .

**Table 5** Selection rule used to enhance the significance for  $H(\rightarrow \gamma\gamma) + E_T^{\text{miss}}$  final state.

Signal region	Cuts
ATLAS signal region	$p_T^{\gamma\gamma} > 90$ GeV, $S_{E_T^{\text{miss}}} > 7$ .
Tight selection	$p_T^{\gamma\gamma} > 90$ GeV, $S_{E_T^{\text{miss}}} > 7$ , $E_T^{\text{miss}} > 200$ GeV, $p_T^\gamma(\text{lead}) > 40$ GeV

At  $\sqrt{s} = 14$  TeV, we can see from Table 3 that the signal-to-background ratio ( $S/B$ ) can go from  $\simeq 10^{-5}$  (after the first selection) to about  $\simeq 1$  in the mono-Higgs signal region. Besides, the efficiency of the signal for  $m_{H^0} = 100$  GeV is  $A \times \epsilon \simeq 25\%$  in the ATLAS signal region. For the FCC-hh at 100 TeV, the signal-to-background ratio can go up to  $\simeq 0.24$  in the tight signal region. If one requires, in addition to the tight selection rules, that  $p_T^\gamma > 60$  GeV (for the leading photon) and  $p_T^\gamma > 50$  GeV (for the sub-leading photon), the significance can increase to around  $\simeq 20$  but the statistics goes down by about an order of magnitude.

## 5 Results and Discussion

In Figs. 9 and 10, we display the normalized distributions for some key observables used in the signal-to-background optimization. We can see that the  $p_T^\gamma$  of the leading photon is stronger for the signal than in the backgrounds with a slightly high peak value for the signal case. The transverse momentum of the diphoton system (top right panel of Figs. 9 and 10) is a good discriminator. This is can be understood as follows; the *Higgs candidate* (reconstructed from the two photons) is produced in association with heavy particles (resulting in a hard missing transverse energy spectrum) and therefore the corresponding recoil imply a harder  $p_T$  than in the backgrounds (especially SM Higgs backgrounds and  $\gamma\gamma$ +jets). The same observation applies to the  $E_T^{\text{miss}}$  (bottom left panel). The  $S_{E_T^{\text{miss}}}$  shows a very important discriminatory power between the signal and the backgrounds. The condition used by the ATLAS collaboration to define the mono-Higgs signal region ( $S_{E_T^{\text{miss}}} > 7$ ) can be considered as an optimum. This is clear because requiring higher values for  $S_{E_T^{\text{miss}}}^{\text{min}}$  will not only reduce the backgrounds but also diminish the signal. We report on a difference between the results of our work and those in the ATLAS paper regarding the  $S_{E_T^{\text{miss}}}$  and  $p_T^{\gamma\gamma}$

<sup>6</sup>A primary vertex is defined as the spatial point where proton-proton collisions occur.

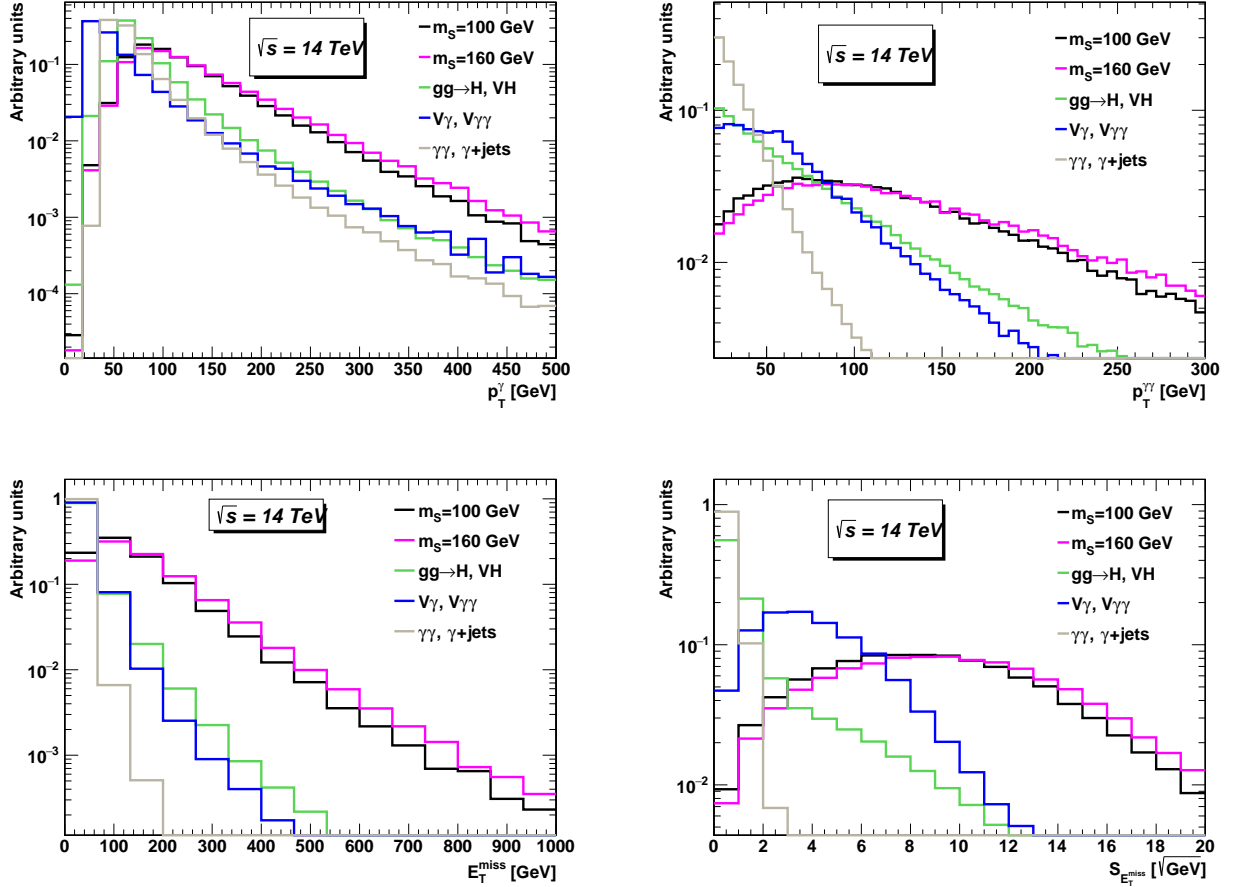


**Fig. 9** Normalized distributions for the signal and the backgrounds at  $\sqrt{s} = 14$  TeV. Here, we show the transverse momentum of the leading photon  $p_T^\gamma$  (top left), the transverse momentum of the diphoton system  $p_T^{\gamma\gamma}$  (top right), missing transverse energy  $E_T^{\text{miss}}$  (bottom left) and the  $S_{E_T^{\text{miss}}}$  defined in eq.(21) (bottom right). The color coding is as follows; SM Higgs processes are shown in green,  $V\gamma$  and  $V\gamma\gamma$  are shown in blue,  $\gamma\gamma$ +jets are shown in gray. We show here the signal for  $m_{H^0} = 100$  GeV (black) and  $m_{H^0} = 160$  GeV (rose).

variables; in the ATLAS paper,  $\gamma\gamma$  and  $\gamma$ +jets events can still have some contribution to these variables (in the hard region) due to the presence of pile-up events (which are not taken into account in our analysis). However, the number of events is still not very important; e.g. about 10 events for  $S_{E_T^{\text{miss}}} > 7$  at  $\sqrt{s} = 13$  TeV and  $\mathcal{L} = 36.5 \text{ fb}^{-1}$ . We can assign the differences in the modeling to an additional systematic uncertainty (see below).

To quantify the discovery potential of the signal, we estimate the significance defined by [133, 134]

$$S = \sqrt{2} \left[ (s+b) \log \left( \frac{(s+b)(b+\delta_b^2)}{b^2 + (s+b)\delta_b^2} \right) - \frac{b^2}{\delta_b^2} \log \left( 1 + \frac{\delta_b^2 s}{b(b+\delta_b^2)} \right) \right]^{1/2}, \quad (22)$$

where  $s$  and  $b$  refer to the number of signal and background events respectively, and  $\delta_b = xb$  is the uncertainty on the background events. Before discussing the results of our sensitivity projections, we comment on the possible sources of systematic uncertainties and their impact on background contribution. First, there are uncertainties related to missing higher order corrections and  $\text{PDF}+\alpha_s$ . Uncertainties due to scale variations are usually determined by varying the renormalization and factorization by a factor of 2 in two directions resulting in an envelope composed of nine possible variations (assuming no correlations with the PDF uncertainties). These uncertainties on the SM Higgs backgrounds are small due to the high precise calculations (2.5-6% for  $m_{\gamma\gamma}/\text{GeV} \in [110 : 160]$ ). Following the recommendation of PDF4LHC working group [135],  $\text{PDF}+\alpha_s$  uncertainties can be estimated by combining both the variations of



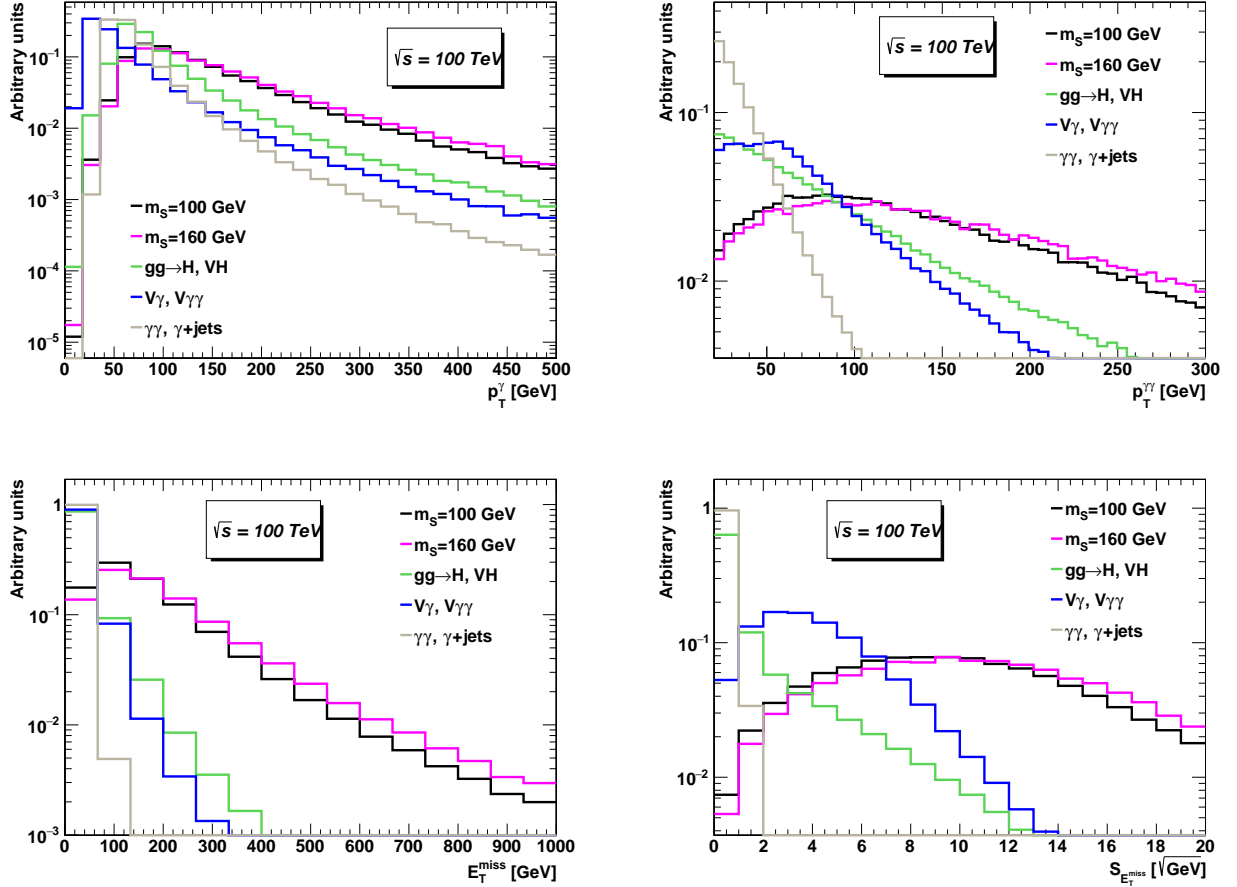


Fig. 10 Same as in Fig. 9 but for  $\sqrt{s} = 100$  TeV.

the same PDF set (used in the calculation of the cross section) with the variations due to alternative PDFs<sup>7</sup>. The size of the envelope spanned by all the variations define the uncertainty due to PDF+ $\alpha_s$ . In the signal region, such uncertainties are very small for SM Higgs backgrounds and can be of order 1.2-2.5% [66]. An additional component of the theory uncertainty comes from the calculations of  $H \rightarrow \gamma\gamma$  branching ratio which is of order 1.73% [136]. The uncertainties on the non-resonant backgrounds can be larger than on the resonant backgrounds. In the analysis of [66], they were estimated directly from data and were of order 0.1-9.8% in the  $110 < m_{\gamma\gamma}/\text{GeV} < 160$  region. On the other hand, there are three major experimental uncertainties in the  $\gamma\gamma + E_T^{\text{miss}}$  final state; Luminosity, Photon identification efficiency and pileup reweighting. The total uncertainty on the background contribution including both resonant and non-resonant processes was estimated by the ATLAS collaboration to be about 15%<sup>8</sup>. In this work, we compute the signal significance taking into account statistical uncertainty only or statistical uncertainty in addition to a systematic uncertainty of order 5%, 10% and 20%.

In Fig. 11, we plot the significance of the signal process at  $\mathcal{L} = 3000 \text{ fb}^{-1}$  as a function of the dark Higgs mass  $m_{H^0}$  for both the HL-LHC and FCC-hh. We show the significance in the ATLAS mono-Higgs signal region (left panels) and in the signal region defined in our paper by the tight selection (right panels). We can see that masses up to 140 (160) GeV can be probed at the LHC (FCC-hh) if one assumes a 5% of total error.

<sup>7</sup>according to the recommendations of PDF4LHC, the central PDF set is NNPDF30 while the two alternatives are CT10 and MMHT

<sup>8</sup>The ATLAS collaboration reported on the total error without specifying the contribution of systematic uncertainties. However, the CMS collaboration [71] reported both the contribution of the statistical error which is the dominant one and the systematic error to the total uncertainty. In the signal region (defined as the High- $p_T^{\text{miss}}$  in the CMS paper), the total systematic uncertainty is  $\simeq 1.6\%$ .

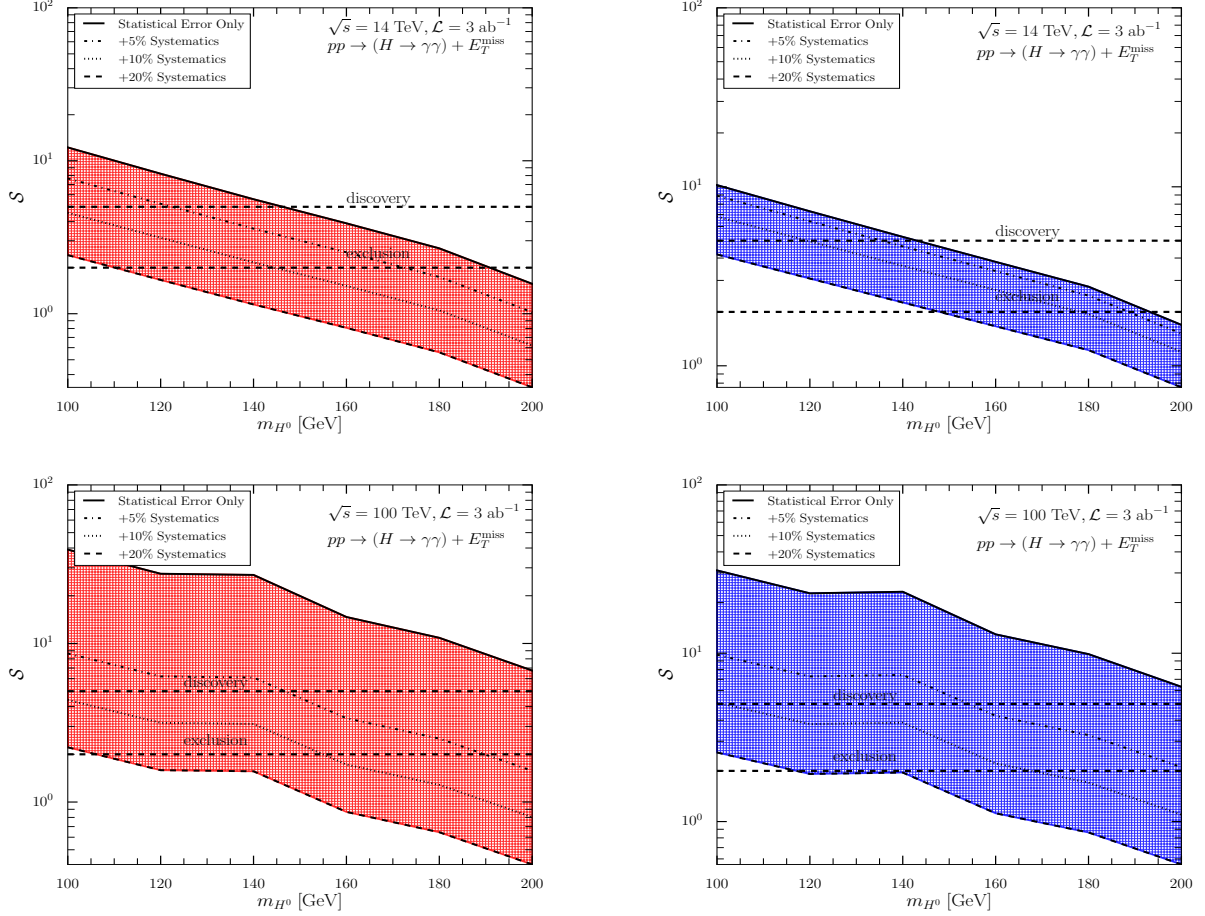


**Fig. 11** Signal significance as a function of the dark Higgs mass  $m_{H^0}$  at  $\int dt \mathcal{L} = 3000 \text{ fb}^{-1}$  in the ATLAS mono-Higgs signal region (left panels) and after the tight selection (right panels) for the LHC at  $\sqrt{s} = 14 \text{ TeV}$  (top panels) and for the FCC-hh at  $\sqrt{s} = 100 \text{ TeV}$  (bottom panels). In all the panels, the solid line corresponds to the significance with the inclusion of the statistical uncertainty only while dot-dashed, dotted and dashed lines include a 5%, 10% and 20% systematic uncertainty (summed in quadrature with the statistical error in the corresponding signal region).

## 6 Conclusions and Outlook

In this work, we carried out a complete study of the mono-Higgs signature in the scotogenic model in the limit of degenerate scalars with a focus on the  $\gamma\gamma$  final state at both the LHC-HL and FCC-hh. After revisiting the collider constraints from LEP and LHC run-II, we have shown that a considerable region of the parameter space is still allowed which is already excluded in general scenarios. Using the most significant benchmark points, we have shown that this model can be probed at the LHC-HL and the FCC-hh in the  $H(\rightarrow \gamma\gamma) + E_T^{\text{miss}}$  channel with  $3 \text{ ab}^{-1}$  of integrated luminosity. The final state we considered has a small rate compared to the other production mechanisms of Majorana DM in the model, however, due to the cleanliness of the  $\gamma\gamma$  decay channel and the high efficiency of photon identification at hadron colliders, we have shown that it can be used to probe the model with the compressed spectrum. In summary, we have found that scalar masses up to 150 (160) GeV can be probed at the LHC (FCC-hh) assuming a 5% systematic uncertainty. We stress out, however, that these results can be significantly improved by the use of multivariate techniques such as boosted decision tree or neural networks and, by including other decay channels of the SM Higgs boson with larger branching fractions. We point out that the importance of the Mono-Higgs signature to probe the scalar coupling  $\lambda_L$  which can't be probed using e.g. mono-jet searches of DM.

In the limit of compressed spectrum, i.e., for  $\lambda_5 \simeq 0$ ; and for  $m_{H^\pm} = 95 \text{ GeV}$ , the dark scalars decay exclusively to a SM lepton (charged lepton or neutrino) and a Majorana fermion. Therefore, the mono-Higgs analysis itself

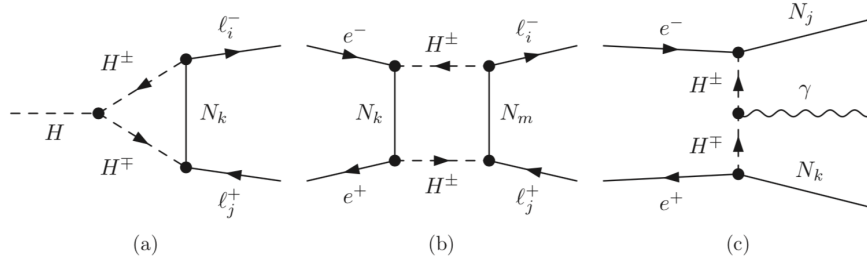


**Fig. 12** Feynman diagrams of processes sensitive to the new Yukawa couplings. we show here the  $H \rightarrow \ell_i \ell_j$ ,  $i \neq j$  (diagram a), the one-loop induced  $e^+ e^- \rightarrow \ell_i^+ \ell_j^-$  (diagram b) and an example of direct production of Majorana fermions (diagram c).

is blind to the absolute values of the new Yukawa couplings as well as to the number of Majorana fermions with mass below the scalar dark Higgs ( $m_{N_k} < m_{H^0}$ ). This conclusion can apply to all the production channels of dark scalars at hadron colliders. It is worth to investigate the potential of other channels and observables to pin down such parameters. Below, we discuss briefly some methods to determine the new Yukawa couplings:

- *Higgs flavor violating decays.* The SM Higgs boson is expected to undergo lepton flavor violating decays in the scotogenic model. These decays are one-loop induced with the exchange of a charged scalar and Majorana fermions (Fig. 12-a). The ATLAS and the CMS collaborations have been searched for these decays channels at  $\sqrt{s} = 8 \oplus 13$  TeV (see e.g. [137, 138]). The null results were used to put severe limits on the LFV Higgs decays, i.e  $\text{BR}(H \rightarrow \mu\tau) < 0.25\%$  and  $\text{BR}(H \rightarrow e\tau) < 0.61\%$  [138]. Possibly observing one or more of these decays channels can be used to constrain one or several combinations of the new Yukawa coupling (These processes are also quadratically dependent on  $g_{HH^\pm H^\pm} \propto \lambda_3$  which can still have large values).
- *Precision measurement of lepton pair production at Lepton Colliders.* In the scotogenic model, a pair of charged leptons ( $e^+ e^- \rightarrow \ell_i^+ \ell_j^-$ ) can be produced with decent rate at center-of-mass energies below or above the  $Z$ -boson pole (Fig. 12-b). Of these processes, the ones with  $i \neq j$  are particularly interesting since they have almost zero cross section in the SM. Therefore, measurement of both inclusive as well as differential rates in  $\ell_i^+ \ell_j^-$  can be used to extract several combinations of the new Yukawa couplings.
- *Direct production at lepton colliders.* The production of inert scalars and Majorana fermions are the most sensitive channels on the new Yukawa couplings (They can also be used as a model discriminators, see e.g. [139]). Production of Majorana fermions (in association with photons, leptons or  $Z$ -bosons) either in the prompt mode or from the decays of dark scalars is possible in the scotogenic model (in Fig. 12-c we display an example of a Feynman diagram for  $N_j N_k \gamma$  production).

**Acknowledgements** A. Ahriche is supported by the Algerian Ministry of Higher Education and Scientific Research under the PRFU Project No B00L02UN180120190003. A. Jueid would like to thank Robert V. Harlander for useful discussions, S. Banerjee for his help regarding the use of DELPHES and F. Siegert for providing the correct setup of the calculation of the  $\gamma$ +jets cross section in SHERPA. The work of A. Arhrib was supported by the Moroccan Ministry of Higher Education and Scientific Research MESRSFC and CNRST: "Projet dans les domaines prioritaires de la recherche scientifique et du développement technologique": PPR/2015/6. The work of AJ is sponsored by CEPC theory program and by the National Natural Science Foundation of China under the Grants No. 11875189 and No.11835005. A. de la Puente would like to thank the ICTP for support where part of this work has been done. The Feynman diagrams are draw using JAXODRAW [140, 141] and FEYNARTS [142].

## Appendix A: Recasting of LHC searches of new physics at $\sqrt{s} = 13$ TeV

In section 3, we studied the impact of the LHC searches of new physics beyond the SM on the parameter space of the compressed scotogenic model. We discuss here the phenomenological setup of the event generation and a brief

description of the analyses used in the reinterpretation effort. These analyses, implemented in CHECKMATE, are listed in Table 1.

- atlas\_conf\_2016\_050 [97]: the ATLAS collaboration has been searched for new phenomena in the final state consisting of  $1 \ell + (b)\text{jets} + E_T^{\text{miss}}$  at  $13.3 \text{ fb}^{-1}$  of luminosity. These searches were focused on the supersymmetric partner of the top quark, and also on DM production in association with a pair of top quarks. Upper bounds on the stop quark mass (for different assumptions regarding its decay branching ratios) were put. Furthermore, limits on DM simplified models were obtained and presented on a plane of DM mass and pseudo-scalar mediator mass for a coupling  $g_{DM} = 3.5$ .
- atlas\_conf\_2016\_066 [98]: Using a dataset corresponding to  $13.3 \text{ fb}^{-1}$  of luminosity, searches of new physics in the final state consisting of one photon, jets and large  $E_T^{\text{miss}}$  is performed by the ATLAS collaboration. These searches were used to probe supersymmetric models with gauge-mediated supersymmetry breaking, where neutralinos decay into a photon and a gravitino. Limits were put on the mass of a degenerate gluino state; i.e.  $m_{\tilde{g}} > 1800 \text{ GeV}$  for a large range of neutralino (the Next-to-Lightest Supersymmetric Particle -NLSP- which is a mixture of higgsino and bino) masses and  $m_{\tilde{g}} > 2000 \text{ GeV}$  for high neutralino mass.
- atlas\_conf\_2016\_076 [99]: A search of stop pair production and DM production in association with  $t\bar{t}$  has been performed using  $13.3 \text{ fb}^{-1}$  of integrated luminosity. This search targeted final states composed of 2 charged leptons, jets and large  $E_T^{\text{miss}}$ . From the non-observation of a beyond the SM signal, 95% CL model-independent upper limits on the visible cross section were obtained (they vary between  $0.38 \text{ fb}$  and  $1.18 \text{ fb}$  depending on the analysis strategy).
- atlas\_conf\_2017\_060 [100]: Using a larger dataset corresponding to  $36.1 \text{ fb}^{-1}$ , a search for new physics in the mono-jet final state ( $1 \text{ jet} + E_T^{\text{miss}}$ ) is performed. Good agreement with the SM expectation was observed. As a consequence, exclusion limits on different models (with pair-produced weakly interacting DM candidates, large extra dimensions, and SUSY particles in several compressed scenarios) were obtained.
- atlas\_1704\_03848 [101]: A search for new physics in the mono-photon final state ( $1 \gamma + E_T^{\text{miss}}$ ) with dataset corresponding to  $\mathcal{L} = 36.1 \text{ fb}^{-1}$  was performed. 95% CL limits were put on models with  $s$ -channel pseudo-scalar mediators, effective field theory models and on the production of a heavy  $Z'$  decaying into  $Z(\rightarrow \nu\nu) + \gamma$ .
- atlas\_1709\_04183 [102]: A search of a stop pair production was performed using the final state  $0 \ell + (n \geq 4) \text{ jets} + E_T^{\text{miss}}$  at luminosity  $36.1 \text{ fb}^{-1}$ . The null searches were used to put exclusions limits on the top-squark and neutralino masses.
- atlas\_1712\_02332 [102]: The final state consisting of (2-6) jets  $+ E_T^{\text{miss}}$  at the luminosity  $36.1 \text{ fb}^{-1}$  recorded by the ATLAS detector, was used to search for squarks and gluinos. 95% CL lower limits on gluino masses ( $m_{\tilde{g}} > 2.03 \text{ TeV}$ ) and squark masses ( $m_{\tilde{q}} > 1.55 \text{ TeV}$ ) were placed.
- atlas\_1712\_08119 [104]: the final states with two low-momentum leptons and missing transverse momentum is used to search for electroweak production of SUSY particles in scenarios with compressed mass spectra at the luminosity  $36.1 \text{ fb}^{-1}$  recorded by ATLAS. Exclusion limits on SUSY particles masses are established.
- atlas\_1802\_03158 [105]: Using  $36.1 \text{ fb}^{-1}$  of luminosity, photonic signatures (single photon and diphoton) in association with large  $E_T^{\text{miss}}$  are considered to look for SUSY particles production in generalized models of gauge-mediated supersymmetry breaking. using  $36.1 \text{ fb}^{-1}$  recorded by ATLAS. In these models, lower limits of 2.15 TeV, 1.82 TeV and 1.06 GeV are set on the masses of gluinos, squarks and a degenerate set of winos, respectively (for any value of the bino mass less than the mass of these produced states).
- cms\_sus\_16\_025 [106]: the final state of two low-momentum opposite-sign leptons and missing transverse momentum in events recorded by CMS at luminosity  $12.9 \text{ fb}^{-1}$  of data collected at 13 TeV, to search for many new physics model candidates. The observed data yields are compatible with the SM predictions, and upper bounds of 175 GeV on charginos and the next-to-lightest neutralino are set, with a mass difference of 7.5 GeV with respect to the lightest neutralino.
- cms\_sus\_16\_039 [107]: Using the data recorded by CMS at 13 TeV and luminosity  $35.9 \text{ fb}^{-1}$ , the final state of multileptons is considered to search for neutralinos and charginos that are weakly produced. In simplified SUSY models, these negative searches were interpreted as exclusions on the mass interval 180-1150 GeV.

- cms\_sus\_16\_048 [108]: Using the same CMS dataset, the final state consisting of two low-momentum, oppositely charged leptons with missing transverse momentum is used to search for new physics. Negative searches results implied exclusions on the wino-like masses up to 230 GeV for 20 GeV mass difference relative to the lightest neutralino, and the higgsino-like masses are excluded up to 168 GeV for the same mass difference. In addition, the top squark masses up to 450 GeV are excluded for a mass difference of 40 GeV relative to the lightest neutralino.

Several processes in the scotogenic model are sensitive to these searches. These processes lead to different final states;  $\ell^+\ell^- + E_T^{\text{miss}}$ ,  $1\gamma + E_T^{\text{miss}}$ , mono-jet, and  $1\ell + \text{jets} + E_T^{\text{miss}}$  among others. First, Charged Higgs boson pair production will lead to a final state composed primarily of 2 isolated charged leptons and a large  $E_T^{\text{miss}}$ . In some cases, where one charged lepton escapes the detection, this final state can be triggered as a  $1\ell + \text{jets} + E_T^{\text{miss}}$  where the jets are produced in initial state radiation. For small mass splittings ( $\Delta_{H^\pm} = m_{H^\pm} - m_{N_k}$ ), the missing transverse energy triggered by the Majorana fermion is even larger and thus gives high sensitivity. Production of a CP-odd (CP-even) dark scalar in association with a charged Higgs boson ( $pp \rightarrow H^0 H^\pm$ ) leads exclusively to  $1\ell + \text{jets} + E_T^{\text{miss}}$ . We also considered the mono- $V$  process with  $V = W, Z$  which contributes to a final state composed of multi-jets ( $n \geq 2$ ) and large transverse missing energy. On the other hand, mono-photon and mono-jet processes are also possible in this model. For mono-jet production, we generated  $S^0 S^0 + n \text{ jets}$  ( $S^0 = H^0, A^0$ ) using MADGRAPH5\_AMC@NLO [117] with jet multiplicity up to 3 jets. We matched these inclusive samples using the MLM matching scheme [143]. PYTHIA 8.155 [144] was used for showering and hadronization. We have added by hand the PDG codes of the three Majorana fermions (which should be considered as invisible particles) to the HCAL modules of the DELPHES card.

## References

1. R. N. Mohapatra and G. Senjanovic, *Neutrino Mass and Spontaneous Parity Violation*, *Phys. Rev. Lett.* **44** (1980) 912. [, 231(1979)].
2. J. Schechter and J. W. F. Valle, *Neutrino Masses in  $SU(2) \times U(1)$  Theories*, *Phys. Rev.* **D22** (1980) 2227.
3. J. Schechter and J. W. F. Valle, *Neutrino Decay and Spontaneous Violation of Lepton Number*, *Phys. Rev.* **D25** (1982) 774.
4. A. Zee, *Charged Scalar Field and Quantum Number Violations*, *Phys. Lett.* **161B** (1985) 141–145.
5. E. Ma, *Pathways to naturally small neutrino masses*, *Phys. Rev. Lett.* **81** (1998) 1171–1174, [[hep-ph/9805219](#)].
6. A. Zee, *Quantum Numbers of Majorana Neutrino Masses*, *Nucl. Phys.* **B264** (1986) 99–110.
7. K. S. Babu, *Model of ‘Calculable’ Majorana Neutrino Masses*, *Phys. Lett.* **B203** (1988) 132–136.
8. M. Aoki, S. Kanemura, T. Shindou, and K. Yagyu, *An  $R$ -parity conserving radiative neutrino mass model without right-handed neutrinos*, *JHEP* **07** (2010) 084, [[arXiv:1005.5159](#)]. [Erratum: JHEP11, 049(2010)].
9. G. Guo, X.-G. He, and G.-N. Li, *Radiative Two Loop Inverse Seesaw and Dark Matter*, *JHEP* **10** (2012) 044, [[arXiv:1207.6308](#)].
10. Y. Kajiyama, H. Okada, and K. Yagyu, *Two Loop Radiative Seesaw Model with Inert Triplet Scalar Field*, *Nucl. Phys.* **B874** (2013) 198–216, [[arXiv:1303.3463](#)].
11. L. M. Krauss, S. Nasri, and M. Trodden, *A Model for neutrino masses and dark matter*, *Phys. Rev.* **D67** (2003) 085002, [[hep-ph/0210389](#)].
12. M. Aoki, S. Kanemura, and O. Seto, *Neutrino mass, Dark Matter and Baryon Asymmetry via TeV-Scale Physics without Fine-Tuning*, *Phys. Rev. Lett.* **102** (2009) 051805, [[arXiv:0807.0361](#)].
13. M. Aoki, S. Kanemura, and O. Seto, *A Model of TeV Scale Physics for Neutrino Mass, Dark Matter and Baryon Asymmetry and its Phenomenology*, *Phys. Rev.* **D80** (2009) 033007, [[arXiv:0904.3829](#)].
14. M. Gustafsson, J. M. No, and M. A. Rivera, *Predictive Model for Radiatively Induced Neutrino Masses and Mixings with Dark Matter*, *Phys. Rev. Lett.* **110** (2013), no. 21 211802, [[arXiv:1212.4806](#)]. [Erratum: Phys. Rev. Lett.112, no.25, 259902(2014)].
15. A. Ahriche, C.-S. Chen, K. L. McDonald, and S. Nasri, *Three-loop model of neutrino mass with dark matter*, *Phys. Rev.* **D90** (2014) 015024, [[arXiv:1404.2696](#)].
16. A. Ahriche, K. L. McDonald, and S. Nasri, *A Model of Radiative Neutrino Mass: with or without Dark Matter*, *JHEP* **10** (2014) 167, [[arXiv:1404.5917](#)].

17. H. Hatanaka, K. Nishiwaki, H. Okada, and Y. Orikasa, *A Three-Loop Neutrino Model with Global  $U(1)$  Symmetry*, *Nucl. Phys.* **B894** (2015) 268–283, [[arXiv:1412.8664](#)].
18. K. Nishiwaki, H. Okada, and Y. Orikasa, *Three loop neutrino model with isolated  $k^{\pm\pm}$* , *Phys. Rev.* **D92** (2015), no. 9 093013, [[arXiv:1507.02412](#)].
19. A. Ahriche, K. L. McDonald, S. Nasri, and T. Toma, *A Model of Neutrino Mass and Dark Matter with an Accidental Symmetry*, *Phys. Lett.* **B746** (2015) 430–435, [[arXiv:1504.05755](#)].
20. A. Ahriche, K. L. McDonald, and S. Nasri, *A Radiative Model for the Weak Scale and Neutrino Mass via Dark Matter*, *JHEP* **02** (2016) 038, [[arXiv:1508.02607](#)].
21. H. Okada and K. Yagyu, *Three-loop neutrino mass model with doubly charged particles from isodoublets*, *Phys. Rev.* **D93** (2016), no. 1 013004, [[arXiv:1508.01046](#)].
22. T. Nomura, H. Okada, and N. Okada, *A Colored KNT Neutrino Model*, *Phys. Lett.* **B762** (2016) 409–414, [[arXiv:1608.02694](#)].
23. P.-H. Gu, *High-scale leptogenesis with three-loop neutrino mass generation and dark matter*, *JHEP* **04** (2017) 159, [[arXiv:1611.03256](#)].
24. K. Cheung, T. Nomura, and H. Okada, *Three-loop neutrino mass model with a colored triplet scalar*, *Phys. Rev.* **D95** (2017), no. 1 015026, [[arXiv:1610.04986](#)].
25. K. Cheung, T. Nomura, and H. Okada, *A Three-loop Neutrino Model with Leptoquark Triplet Scalars*, *Phys. Lett.* **B768** (2017) 359–364, [[arXiv:1701.01080](#)].
26. B. Dutta, S. Ghosh, I. Gogoladze, and T. Li, *Three-loop neutrino masses via new massive gauge bosons from  $E_6$  GUT*, *Phys. Rev.* **D98** (2018), no. 5 055028, [[arXiv:1805.01866](#)].
27. T. Nomura and H. Okada, *Four-loop Neutrino Model Inspired by Diphoton Excess at 750 GeV*, *Phys. Lett.* **B755** (2016) 306–311, [[arXiv:1601.00386](#)].
28. N. G. Deshpande and E. Ma, *Pattern of Symmetry Breaking with Two Higgs Doublets*, *Phys. Rev.* **D18** (1978) 2574.
29. R. Barbieri, L. J. Hall, and V. S. Rychkov, *Improved naturalness with a heavy Higgs: An Alternative road to LHC physics*, *Phys. Rev.* **D74** (2006) 015007, [[hep-ph/0603188](#)].
30. E. Ma, *Verifiable radiative seesaw mechanism of neutrino mass and dark matter*, *Phys. Rev.* **D73** (2006) 077301, [[hep-ph/0601225](#)].
31. M. Gustafsson, E. Lundstrom, L. Bergstrom, and J. Edsjo, *Significant Gamma Lines from Inert Higgs Dark Matter*, *Phys. Rev. Lett.* **99** (2007) 041301, [[astro-ph/0703512](#)].
32. T. Hambye and M. H. G. Tytgat, *Electroweak symmetry breaking induced by dark matter*, *Phys. Lett.* **B659** (2008) 651–655, [[arXiv:0707.0633](#)].
33. P. Agrawal, E. M. Dolle, and C. A. Krenke, *Signals of Inert Doublet Dark Matter in Neutrino Telescopes*, *Phys. Rev.* **D79** (2009) 015015, [[arXiv:0811.1798](#)].
34. E. M. Dolle and S. Su, *The Inert Dark Matter*, *Phys. Rev.* **D80** (2009) 055012, [[arXiv:0906.1609](#)].
35. S. Andreas, M. H. G. Tytgat, and Q. Swillens, *Neutrinos from Inert Doublet Dark Matter*, *JCAP* **0904** (2009) 004, [[arXiv:0901.1750](#)].
36. E. Dolle, X. Miao, S. Su, and B. Thomas, *Dilepton Signals in the Inert Doublet Model*, *Phys. Rev.* **D81** (2010) 035003, [[arXiv:0909.3094](#)].
37. X. Miao, S. Su, and B. Thomas, *Trilepton Signals in the Inert Doublet Model*, *Phys. Rev.* **D82** (2010) 035009, [[arXiv:1005.0090](#)].
38. A. Arhrib, R. Benbrik and N. Gaur, “ $H \rightarrow \gamma\gamma$  in Inert Higgs Doublet Model,” *Phys. Rev. D* **85** (2012) 095021 doi:10.1103/PhysRevD.85.095021 [[arXiv:1201.2644](#) [[hep-ph](#)]].
39. A. Arhrib, Y.-L. S. Tsai, Q. Yuan, and T.-C. Yuan, *An Updated Analysis of Inert Higgs Doublet Model in light of the Recent Results from LUX, PLANCK, AMS-02 and LHC*, *JCAP* **1406** (2014) 030, [[arXiv:1310.0358](#)].
40. A. Goudelis, B. Herrmann, and O. Stål, *Dark matter in the Inert Doublet Model after the discovery of a Higgs-like boson at the LHC*, *JHEP* **09** (2013) 106, [[arXiv:1303.3010](#)].
41. A. Arhrib, R. Benbrik, and T.-C. Yuan, *Associated Production of Higgs at Linear Collider in the Inert Higgs Doublet Model*, *Eur. Phys. J.* **C74** (2014) 2892, [[arXiv:1401.6698](#)].



42. A. Arhrib, R. Benbrik, J. El Falaki, and A. Jueid, *Radiative corrections to the Triple Higgs Coupling in the Inert Higgs Doublet Model*, *JHEP* **12** (2015) 007, [[arXiv:1507.03630](#)].
43. H. Castilla-Valdez, A. Moyotl, M. A. Perez, and C. G. Honorato, *Sensitivity of the decay  $h \rightarrow ZZ^* \rightarrow Zl + l^-$  to the Higgs self-coupling through radiative corrections*, *Phys. Rev.* **D93** (2016), no. 5 055001, [[arXiv:1512.03872](#)].
44. S. Kanemura, M. Kikuchi, and K. Sakurai, *Testing the dark matter scenario in the inert doublet model by future precision measurements of the Higgs boson couplings*, *Phys. Rev.* **D94** (2016), no. 11 115011, [[arXiv:1605.08520](#)].
45. S. Banerjee and N. Chakrabarty, *A revisit to scalar dark matter with radiative corrections*, [arXiv:1612.01973](#).
46. P. Poulose, S. Sahoo, and K. Sridhar, *Exploring the Inert Doublet Model through the dijet plus missing transverse energy channel at the LHC*, *Phys. Lett.* **B765** (2017) 300–306, [[arXiv:1604.03045](#)].
47. F. P. Huang and J.-H. Yu, *Explore Inert Dark Matter Blind Spots with Gravitational Wave Signatures*, [arXiv:1704.04201](#).
48. N. Wan, N. Li, B. Zhang, H. Yang, M.-F. Zhao, M. Song, G. Li, and J.-Y. Guo, *Searches for Dark Matter via Mono- $W$  Production in Inert Doublet Model at the LHC*, *Commun. Theor. Phys.* **69** (2018), no. 5 617.
49. A. Belyaev, T. R. Fernandez Perez Tomei, P. G. Mercadante, C. S. Moon, S. Moretti, S. F. Novaes, L. Panizzi, F. Rojas, and M. Thomas, *Advancing LHC Probes of Dark Matter from the Inert 2-Higgs Doublet Model with the mono-jet Signal*, [arXiv:1809.00933](#).
50. A. Belyaev, G. Cacciapaglia, I. P. Ivanov, F. Rojas-Abatte, and M. Thomas, *Anatomy of the Inert Two Higgs Doublet Model in the light of the LHC and non-LHC Dark Matter Searches*, *Phys. Rev.* **D97** (2018), no. 3 035011, [[arXiv:1612.00511](#)].
51. E. Lundstrom, M. Gustafsson, and J. Edsjo, *The Inert Doublet Model and LEP II Limits*, *Phys. Rev.* **D79** (2009) 035013, [[arXiv:0810.3924](#)].
52. G. Belanger, B. Dumont, A. Goudelis, B. Herrmann, S. Kraml, and D. Sengupta, *Dilepton constraints in the Inert Doublet Model from Run 1 of the LHC*, *Phys. Rev.* **D91** (2015), no. 11 115011, [[arXiv:1503.07367](#)].
53. N. Blinov, J. Kozaczuk, D. E. Morrissey, and A. de la Puente, *Compressing the Inert Doublet Model*, *Phys. Rev.* **D93** (2016), no. 3 035020, [[arXiv:1510.08069](#)].
54. A. Ahriche, A. Jueid, and S. Nasri, *Radiative neutrino mass and Majorana dark matter within an inert Higgs doublet model*, *Phys. Rev.* **D97** (2018), no. 9 095012, [[arXiv:1710.03824](#)].
55. A. Vicente and C. E. Yaguna, *Probing the scotogenic model with lepton flavor violating processes*, *JHEP* **1502**, 144 (2015) doi:10.1007/JHEP02(2015)144 [[arXiv:1412.2545](#) [hep-ph]].
56. A. Merle and M. Platscher, *Parity Problem of the Scotogenic Neutrino Model*, *Phys. Rev.* **D92** (2015), no. 9 095002, [[arXiv:1502.03098](#)].
57. T. Kitabayashi, *Scotogenic dark matter and single-zero textures of the neutrino mass matrix*, *Phys. Rev. D* **98** (2018), no. 8, 083011, [arXiv:1808.01060](#).
58. T. Hugle, M. Platscher, and K. Schmitz, *Low-Scale Leptogenesis in the Scotogenic Neutrino Mass Model*, *Phys. Rev.* **D98** (2018), no. 2 023020, [[arXiv:1804.09660](#)].
59. S. Baumholzer, V. Brdar, and P. Schwaller, *The New  $\nu$ MSM ( $\nu\nu$ MSM): Radiative Neutrino Masses, keV-Scale Dark Matter and Viable Leptogenesis with sub-TeV New Physics*, *JHEP* **08** (2018) 067, [[arXiv:1806.06864](#)].
60. D. Borah, P. S. B. Dev and A. Kumar, *TeV scale leptogenesis, inflaton dark matter and neutrino mass in a scotogenic model*, *Phys. Rev. D* **99** (2019) 055012 doi:10.1103/PhysRevD.99.055012 [[arXiv:1810.03645](#) [hep-ph]].
61. L. Carpenter, A. DiFranzo, M. Mulhearn, C. Shimmin, S. Tulin, and D. Whiteson, *Mono-Higgs-boson: A new collider probe of dark matter*, *Phys. Rev.* **D89** (2014), no. 7 075017, [[arXiv:1312.2592](#)].
62. A. A. Petrov and W. Shepherd, *Searching for dark matter at LHC with Mono-Higgs production*, *Phys. Lett.* **B730** (2014) 178–183, [[arXiv:1311.1511](#)].
63. W. Abdallah, A. Hammad, S. Khalil, and S. Moretti, *Search for Mono-Higgs Signals at the LHC in the B-L Supersymmetric Standard Model*, *Phys. Rev.* **D95** (2017), no. 5 055019, [[arXiv:1608.07500](#)].
64. K. Ghorbani and L. Khalkhali, *Mono-Higgs signature in a fermionic dark matter model*, *J. Phys.* **G44** (2017), no. 10 105004, [[arXiv:1608.04559](#)].
65. ATLAS Collaboration, G. Aad et al., *Search for Dark Matter in Events with Missing Transverse Momentum and a Higgs Boson Decaying to Two Photons in  $pp$  Collisions at  $\sqrt{s} = 8$  TeV with the ATLAS Detector*, *Phys.*



- 
- Rev. Lett.* **115** (2015), no. 13 131801, [[arXiv:1506.01081](#)].
66. **ATLAS** Collaboration, M. Aaboud et al., *Search for dark matter in association with a Higgs boson decaying to two photons at  $\sqrt{s} = 13$  TeV with the ATLAS detector*, *Phys. Rev.* **D96** (2017), no. 11 112004, [[arXiv:1706.03948](#)].
  67. **ATLAS** Collaboration, M. Aaboud et al., *Search for dark matter in association with a Higgs boson decaying to  $b$ -quarks in  $pp$  collisions at  $\sqrt{s} = 13$  TeV with the ATLAS detector*, *Phys. Lett.* **B765** (2017) 11–31, [[arXiv:1609.04572](#)].
  68. **ATLAS** Collaboration, M. Aaboud et al., *Search for Dark Matter Produced in Association with a Higgs Boson Decaying to  $b\bar{b}$  using  $36\text{ fb}^{-1}$  of  $pp$  collisions at  $\sqrt{s} = 13$  TeV with the ATLAS Detector*, *Phys. Rev. Lett.* **119** (2017), no. 18 181804, [[arXiv:1707.01302](#)].
  69. **CMS** Collaboration, A. M. Sirunyan et al., *Search for associated production of dark matter with a Higgs boson decaying to  $b\bar{b}$  or  $\gamma\gamma$  at  $\sqrt{s} = 13$  TeV*, *JHEP* **10** (2017) 180, [[arXiv:1703.05236](#)].
  70. **CMS** Collaboration, A. M. Sirunyan et al., *Search for dark matter produced in association with a Higgs boson decaying to a pair of bottom quarks in proton-proton collisions at  $\sqrt{s} = 13$  TeV*, Submitted to: *Eur. Phys. J.* (2018) [[arXiv:1811.06562](#)].
  71. **CMS** Collaboration, A. M. Sirunyan et al., *Search for dark matter produced in association with a Higgs boson decaying to  $\gamma\gamma$  or  $\tau^+\tau^-$  at  $\sqrt{s} = 13$  TeV*, *JHEP* **09** (2018) 046, [[arXiv:1806.04771](#)].
  72. S. P. Martin, *Two loop effective potential for a general renormalizable theory and softly broken supersymmetry*, *Phys. Rev.* **D65** (2002) 116003, [[hep-ph/0111209](#)].
  73. Y. Cai, J. Herrero-García, M. A. Schmidt, A. Vicente and R. R. Volkas, “From the trees to the forest: a review of radiative neutrino mass models,” *Front. in Phys.* **5** (2017) 63 doi:10.3389/fphy.2017.00063 [[arXiv:1706.08524](#) [hep-ph]].
  74. J. A. Casas and A. Ibarra, *Oscillating neutrinos and  $\mu \rightarrow e, \gamma$* , *Nucl. Phys.* **B618** (2001) 171–204, [[hep-ph/0103065](#)].
  75. B. Pontecorvo, *Neutrino Experiments and the Problem of Conservation of Leptonic Charge*, *Sov. Phys. JETP* **26** (1968) 984–988. [*Zh. Eksp. Teor. Fiz.* 53, 1717(1967)].
  76. D. V. Forero, M. Tortola, and J. W. F. Valle, *Global status of neutrino oscillation parameters after Neutrino-2012*, *Phys. Rev.* **D86** (2012) 073012, [[arXiv:1205.4018](#)].
  77. G. C. Branco, P. M. Ferreira, L. Lavoura, M. N. Rebelo, M. Sher, and J. P. Silva, *Theory and phenomenology of two-Higgs-doublet models*, *Phys. Rept.* **516** (2012) 1–102, [[arXiv:1106.0034](#)].
  78. I. F. Ginzburg, K. A. Kanishev, M. Krawczyk, and D. Sokolowska, *Evolution of Universe to the present inert phase*, *Phys. Rev.* **D82** (2010) 123533, [[arXiv:1009.4593](#)].
  79. S. Kanemura, T. Kubota, and E. Takasugi, *Lee-Quigg-Thacker bounds for Higgs boson masses in a two doublet model*, *Phys. Lett.* **B313** (1993) 155–160, [[hep-ph/9303263](#)].
  80. A. G. Akeroyd, A. Arhrib, and E.-M. Naimi, *Note on tree level unitarity in the general two Higgs doublet model*, *Phys. Lett.* **B490** (2000) 119–124, [[hep-ph/0006035](#)].
  81. M. E. Peskin and T. Takeuchi, *Estimation of oblique electroweak corrections*, *Phys. Rev.* **D46** (1992) 381–409.
  82. W. Grimus, L. Lavoura, O. M. Ogreid, and P. Osland, *The Oblique parameters in multi-Higgs-doublet models*, *Nucl. Phys.* **B801** (2008) 81–96, [[arXiv:0802.4353](#)].
  83. **Particle Data Group** Collaboration, C. Patrignani et al., *Review of Particle Physics*, *Chin. Phys.* **C40** (2016), no. 10 100001.
  84. T. Toma and A. Vicente, *Lepton Flavor Violation in the Scotogenic Model*, *JHEP* **01** (2014) 160, [[arXiv:1312.2840](#)].
  85. **ATLAS** Collaboration, T. A. collaboration, *Combined measurements of Higgs boson production and decay using up to  $80\text{ fb}^{-1}$  of proton-proton collision data at  $\sqrt{s} = 13$  TeV collected with the ATLAS experiment*, .
  86. J. Bernon and B. Dumont, *Lilith: a tool for constraining new physics from Higgs measurements*, *Eur. Phys. J.* **C75** (2015), no. 9 440, [[arXiv:1502.04138](#)].
  87. S. Kraml, T. Q. Loc, D. T. Nhung and L. D. Ninh, “Constraining new physics from Higgs measurements with Lilith: update to LHC Run 2 results,” [arXiv:1908.03952](#) [hep-ph].

88. A. M. Sirunyan *et al.* [CMS Collaboration], “Combined measurements of Higgs boson couplings in proton–proton collisions at  $\sqrt{s} = 13$  TeV, ” *Eur. Phys. J. C* **79** (2019) no.5, 421 doi:10.1140/epjc/s10052-019-6909-y [arXiv:1809.10733 [hep-ex]].
89. **WMAP** Collaboration, G. Hinshaw *et al.*, *Nine-Year Wilkinson Microwave Anisotropy Probe (WMAP) Observations: Cosmological Parameter Results*, *Astrophys. J. Suppl.* **208** (2013) 19, [arXiv:1212.5226].
90. **Planck** Collaboration, P. A. R. Ade *et al.*, *Planck 2015 results. XIII. Cosmological parameters*, *Astron. Astrophys.* **594** (2016) A13, [arXiv:1502.01589].
91. **XENON** Collaboration, E. Aprile *et al.*, *First Dark Matter Search Results from the XENON1T Experiment*, *Phys. Rev. Lett.* **119** (2017), no. 18 181301, [arXiv:1705.06655].
92. S. M. Espirito, H. K. P. Johansson, and A. Lipniacka *DELPHI-002 PHYS 928* (2003).
93. **OPAL** Collaboration, G. Abbiendi *et al.*, *Search for anomalous production of dilepton events with missing transverse momentum in  $e^+e^-$  collisions at  $s^{1/2} = 183$ -GeV to 209-GeV*, *Eur. Phys. J.* **C32** (2004) 453–473, [hep-ex/0309014].
94. **OPAL** Collaboration, G. Abbiendi *et al.*, *Search for chargino and neutralino production at  $s^{1/2} = 192$ -GeV to 209 GeV at LEP*, *Eur. Phys. J.* **C35** (2004) 1–20, [hep-ex/0401026].
95. **DELPHI** Collaboration, J. Abdallah *et al.*, *Searches for supersymmetric particles in  $e^+e^-$  collisions up to 208-GeV and interpretation of the results within the MSSM*, *Eur. Phys. J.* **C31** (2003) 421–479, [hep-ex/0311019].
96. A. Pierce and J. Thaler, *Natural Dark Matter from an Unnatural Higgs Boson and New Colored Particles at the TeV Scale*, *JHEP* **08** (2007) 026, [hep-ph/0703056].
97. **ATLAS** Collaboration, T. A. collaboration, *Search for top squarks in final states with one isolated lepton, jets, and missing transverse momentum in  $\sqrt{s} = 13$  TeV pp collisions with the ATLAS detector*, .
98. **ATLAS** Collaboration, T. A. collaboration, *Search for Supersymmetry in events with photons, jets and missing transverse energy with the ATLAS detector in 13 TeV pp collisions*, .
99. **ATLAS** Collaboration, T. A. collaboration, *Search for direct top squark pair production and dark matter production in final states with two leptons in  $\sqrt{s} = 13$  TeV pp collisions using  $13.3 \text{ fb}^{-1}$  of ATLAS data*, .
100. **ATLAS** Collaboration, T. A. collaboration, *Search for dark matter and other new phenomena in events with an energetic jet and large missing transverse momentum using the ATLAS detector*, .
101. **ATLAS** Collaboration, M. Aaboud *et al.*, *Search for dark matter at  $\sqrt{s} = 13$  TeV in final states containing an energetic photon and large missing transverse momentum with the ATLAS detector*, *Eur. Phys. J.* **C77** (2017), no. 6 393, [arXiv:1704.03848].
102. **ATLAS** Collaboration, M. Aaboud *et al.*, *Search for a scalar partner of the top quark in the jets plus missing transverse momentum final state at  $\sqrt{s}=13$  TeV with the ATLAS detector*, *JHEP* **12** (2017) 085, [arXiv:1709.04183].
103. **ATLAS** Collaboration, M. Aaboud *et al.*, *Search for squarks and gluinos in final states with jets and missing transverse momentum using  $36.1 \text{ fb}^{-1}$  of  $\sqrt{s} = 13 \text{ TeV}$  pp collision data with the ATLAS detector*, *Phys. Rev.* **D97** (2018), no. 11 112001, [arXiv:1712.02332].
104. **ATLAS** Collaboration, M. Aaboud *et al.*, *Search for electroweak production of supersymmetric states in scenarios with compressed mass spectra at  $\sqrt{s} = 13$  TeV with the ATLAS detector*, *Phys. Rev.* **D97** (2018), no. 5 052010, [arXiv:1712.08119].
105. **ATLAS** Collaboration, M. Aaboud *et al.*, *Search for photonic signatures of gauge-mediated supersymmetry in 13 TeV pp collisions with the ATLAS detector*, *Phys. Rev.* **D97** (2018), no. 9 092006, [arXiv:1802.03158].
106. **CMS** Collaboration, C. Collaboration, *Search for new physics in the compressed mass spectra scenario using events with two soft opposite-sign leptons and missing momentum energy at 13 TeV*, .
107. **CMS** Collaboration, A. M. Sirunyan *et al.*, *Search for electroweak production of charginos and neutralinos in multilepton final states in proton-proton collisions at  $\sqrt{s} = 13$  TeV*, *JHEP* **03** (2018) 166, [arXiv:1709.05406].
108. **CMS** Collaboration, A. M. Sirunyan *et al.*, *Search for new physics in events with two soft oppositely charged leptons and missing transverse momentum in proton-proton collisions at  $\sqrt{s} = 13$  TeV*, *Phys. Lett.* **B782** (2018) 440–467, [arXiv:1801.01846].

109. M. L. Graesser and J. Shelton, *Hunting Mixed Top Squark Decays*, *Phys. Rev. Lett.* **111** (2013), no. 12 121802, [[arXiv:1212.4495](#)].
110. M. Drees, H. Dreiner, D. Schmeier, J. Tattersall, and J. S. Kim, *CheckMATE: Confronting your Favourite New Physics Model with LHC Data*, *Comput. Phys. Commun.* **187** (2015) 227–265, [[arXiv:1312.2591](#)].
111. M. R. Buckley, J. D. Lykken, C. Rogan, and M. Spiropulu, *Super-Razor and Searches for Sleptons and Charginos at the LHC*, *Phys. Rev.* **D89** (2014), no. 5 055020, [[arXiv:1310.4827](#)].
112. D. Dercks, N. Desai, J. S. Kim, K. Rolbiecki, J. Tattersall, and T. Weber, *CheckMATE 2: From the model to the limit*, *Comput. Phys. Commun.* **221** (2017) 383–418, [[arXiv:1611.09856](#)].
113. J. S. Kim, D. Schmeier, J. Tattersall, and K. Rolbiecki, *A framework to create customised LHC analyses within CheckMATE*, *Comput. Phys. Commun.* **196** (2015) 535–562, [[arXiv:1503.01123](#)].
114. R. V. Harlander, S. Liebler, and H. Mantler, *SusHi: A program for the calculation of Higgs production in gluon fusion and bottom-quark annihilation in the Standard Model and the MSSM*, *Comput. Phys. Commun.* **184** (2013) 1605–1617, [[arXiv:1212.3249](#)].
115. R. V. Harlander, S. Liebler, and H. Mantler, *SusHi Bento: Beyond NNLO and the heavy-top limit*, *Comput. Phys. Commun.* **212** (2017) 239–257, [[arXiv:1605.03190](#)].
116. O. Brein, R. V. Harlander, and T. J. E. Zirke, *vh@nnlo - Higgs Strahlung at hadron colliders*, *Comput. Phys. Commun.* **184** (2013) 998–1003, [[arXiv:1210.5347](#)].
117. J. Alwall, R. Frederix, S. Frixione, V. Hirschi, F. Maltoni, O. Mattelaer, H. S. Shao, T. Stelzer, P. Torrielli, and M. Zaro, *The automated computation of tree-level and next-to-leading order differential cross sections, and their matching to parton shower simulations*, *JHEP* **07** (2014) 079, [[arXiv:1405.0301](#)].
118. T. Gleisberg, S. Höche, F. Krauss, M. Schönherr, S. Schumann, F. Siegert, and J. Winter, *Event generation with SHERPA 1.1*, *JHEP* **02** (2009) 007, [[arXiv:0811.4622](#)].
119. K. G. Chetyrkin, J. H. Kuhn, and M. Steinhauser, *RunDec: A Mathematica package for running and decoupling of the strong coupling and quark masses*, *Comput. Phys. Commun.* **133** (2000) 43–65, [[hep-ph/0004189](#)].
120. R. V. Harlander and W. B. Kilgore, *Next-to-next-to-leading order Higgs production at hadron colliders*, *Phys. Rev. Lett.* **88** (2002) 201801, [[hep-ph/0201206](#)].
121. C. Anastasiou, C. Duhr, F. Dulat, E. Furlan, T. Gehrmann, F. Herzog, and B. Mistlberger, *Higgs Boson GluonFusion Production Beyond Threshold in  $N^3LO$  QCD*, *JHEP* **03** (2015) 091, [[arXiv:1411.3584](#)].
122. C. Anastasiou, C. Duhr, F. Dulat, E. Furlan, F. Herzog, and B. Mistlberger, *Soft expansion of double-real-virtual corrections to Higgs production at  $N^3LO$* , *JHEP* **08** (2015) 051, [[arXiv:1505.04110](#)].
123. C. Anastasiou, C. Duhr, F. Dulat, E. Furlan, T. Gehrmann, F. Herzog, A. Lazopoulos, and B. Mistlberger, *High precision determination of the gluon fusion Higgs boson cross-section at the LHC*, *JHEP* **05** (2016) 058, [[arXiv:1602.00695](#)].
124. O. Brein, A. Djouadi, and R. Harlander, *NNLO QCD corrections to the Higgs-strahlung processes at hadron colliders*, *Phys. Lett.* **B579** (2004) 149–156, [[hep-ph/0307206](#)].
125. M. L. Ciccolini, S. Dittmaier, and M. Kramer, *Electroweak radiative corrections to associated WH and ZH production at hadron colliders*, *Phys. Rev.* **D68** (2003) 073003, [[hep-ph/0306234](#)].
126. O. Brein, R. Harlander, M. Wiesemann, and T. Zirke, *Top-Quark Mediated Effects in Hadronic Higgs-Strahlung*, *Eur. Phys. J.* **C72** (2012) 1868, [[arXiv:1111.0761](#)].
127. J. Gao, M. Guzzi, J. Huston, H.-L. Lai, Z. Li, P. Nadolsky, J. Pumplin, D. Stump, and C. P. Yuan, *CT10 next-to-next-to-leading order global analysis of QCD*, *Phys. Rev.* **D89** (2014), no. 3 033009, [[arXiv:1302.6246](#)].
128. NNPDF Collaboration, R. D. Ball et al., *Parton distributions for the LHC Run II*, *JHEP* **04** (2015) 040, [[arXiv:1410.8849](#)].
129. S. Catani, F. Krauss, R. Kuhn, and B. R. Webber, *QCD matrix elements + parton showers*, *JHEP* **11** (2001) 063, [[hep-ph/0109231](#)].
130. T. Sjöstrand, S. Ask, J. R. Christiansen, R. Corke, N. Desai, P. Ilten, S. Mrenna, S. Prestel, C. O. Rasmussen, and P. Z. Skands, *An Introduction to PYTHIA 8.2*, *Comput. Phys. Commun.* **191** (2015) 159–177, [[arXiv:1410.3012](#)].
131. DELPHES 3 Collaboration, J. de Favereau, C. Delaere, P. Demin, A. Giammanco, V. Lemaître, A. Mertens, and M. Selvaggi, *DELPHES 3, A modular framework for fast simulation of a generic collider experiment*, *JHEP*

- 02** (2014) 057, [[arXiv:1307.6346](#)].
132. M. Mangano, *Physics at the FCC-hh, a 100 TeV pp collider*, *CERN Yellow Rep. Monogr.* **3** (2017) [[arXiv:1710.06353](#)].
  133. G. Cowan, K. Cranmer, E. Gross, and O. Vitells, *Asymptotic formulae for likelihood-based tests of new physics*, *Eur. Phys. J.* **C71** (2011) 1554, [[arXiv:1007.1727](#)]. [Erratum: *Eur. Phys. J.* **C73**, 2501(2013)].
  134. B. Coleppa, B. Fuks, P. Poulose, and S. Sahoo, *Seeking Heavy Higgs Bosons through Cascade Decays*, *Phys. Rev.* **D97** (2018), no. 7 075007, [[arXiv:1712.06593](#)].
  135. J. Butterworth *et al.*, *PDF4LHC recommendations for LHC Run II*, *J. Phys. G* **43** (2016) 023001 doi:10.1088/0954-3899/43/2/023001 [[arXiv:1510.03865](#) [hep-ph]].
  136. D. de Florian *et al.* [LHC Higgs Cross Section Working Group], *Handbook of LHC Higgs Cross Sections: 4. Deciphering the Nature of the Higgs Sector*, doi:10.23731/CYRM-2017-002 [arXiv:1610.07922](#) [hep-ph].
  137. G. Aad *et al.* [ATLAS Collaboration], *Search for lepton-flavour-violating decays of the Higgs and Z bosons with the ATLAS detector*, *Eur. Phys. J. C* **77** (2017) no.2, 70 doi:10.1140/epjc/s10052-017-4624-0 [[arXiv:1604.07730](#) [hep-ex]].
  138. A. M. Sirunyan *et al.* [CMS Collaboration], *Search for lepton flavour violating decays of the Higgs boson to  $\mu\tau$  and  $e\tau$  in proton-proton collisions at  $\sqrt{s} = 13$  TeV*, *JHEP* **1806** (2018) 001 doi:10.1007/JHEP06(2018)001 [[arXiv:1712.07173](#) [hep-ex]].
  139. I. Maturana-Ãvila, M. A. DÃaz, N. Rojas and S. Urrutia-Quiroga, *Towards a way to distinguish between IHDM and the Scotogenic at CLIC*, [arXiv:1903.11181](#) [hep-ph].
  140. D. Binosi and L. Theussl, *JaxoDraw: A Graphical user interface for drawing Feynman diagrams*, *Comput. Phys. Commun.* **161** (2004) 76 doi:10.1016/j.cpc.2004.05.001 [hep-ph/0309015].
  141. D. Binosi, J. Collins, C. Kaufhold and L. Theussl, *JaxoDraw: A Graphical user interface for drawing Feynman diagrams. Version 2.0 release notes*, *Comput. Phys. Commun.* **180** (2009) 1709 doi:10.1016/j.cpc.2009.02.020 [[arXiv:0811.4113](#) [hep-ph]].
  142. T. Hahn, *Generating Feynman diagrams and amplitudes with FeynArts 3*, *Comput. Phys. Commun.* **140** (2001) 418 doi:10.1016/S0010-4655(01)00290-9 [hep-ph/0012260].
  143. M. L. Mangano, M. Moretti, F. Piccinini and M. Treccani, *Matching matrix elements and shower evolution for top-quark production in hadronic collisions*, *JHEP* **0701** (2007) 013 doi:10.1088/1126-6708/2007/01/013 [hep-ph/0611129].
  144. T. Sjostrand, S. Mrenna and P. Z. Skands, *A Brief Introduction to PYTHIA 8.1*, *Comput. Phys. Commun.* **178** (2008) 852 doi:10.1016/j.cpc.2008.01.036 [[arXiv:0710.3820](#) [hep-ph]].
  145. H. K. Dreiner, M. Kramer and J. Tattersall, *How low can SUSY go? Matching, monojets and compressed spectra*, *EPL* **99** (2012) no.6, 61001 doi:10.1209/0295-5075/99/61001 [[arXiv:1207.1613](#) [hep-ph]].